Journal of Mechanics Engineering and Automation 2 (2012) 606-627

Static Stability Analysis of a Single Planar Object Grasped by a Multifingered Hand

Takayoshi Yamada[1], Manabu Yamada[2] and Hidehiko Yamamoto[1]

1. Department of Human and Information Systems, Faculty of Engineering, Gifu University, Gifu 501-1193, Japan

2. Department of Mechanical Engineering, Faculty of Engineering, Nagoya Institute of Technology, Nagoya 466-8555, Japan

Received: September 17, 2012 / Accepted: October 16, 2012 / Published: October 25, 2012.

Abstract: In this study, the static stability of the grasp of a single planar object is analyzed using the potential energy method. In previous papers, we considered cases in which individual fingers were replaced by a multidimensional translational spring model, in which each finger is constructed with prismatic joints. Human hands and the most developed mechanical hands are constructed with revolute joints. In this paper, the effects of fingertip rotation and a revolute joint spring model are investigated. A grasp stiffness matrix is analytically derived by considering not only frictional rolling contact but also frictionless sliding contact. The difference between the frictional stiffness matrix and the frictionless one is analytically obtained. The effect of local curvature at contact points is analytically derived. The grasp displacement directions affected by the change in curvature and the contact condition are also obtained. The derived stiffness matrix of the revolute joint model is compared with that of the prismatic joint model, and then the stiffness relation is clarified. The gravity effect of the object is also considered. The effectiveness of our method is demonstrated through numerical examples. The stability is evaluated by the eigenvalues of the grasp stiffness matrix, and the grasp displacement direction is obtained by the corresponding eigenvectors. The effect of joint angle is also discussed.

Key words: Grasping, multifingered hands, static grasp stability, revolute joint stiffness model.

1. Introduction

Human beings, especially magicians and jugglers, easily manipulate multiple objects using their dexterous hands. Multifingered robot hands are also potentially capable of performing similar manipulations.

During these manipulations, grasp stability is an important factor. Hanafusa and Asada [1] investigated the stability of planar grasping using frictionless elastic fingers and observed that a stable grasp is obtained using the potential energy stored in the grasp. Nguyen [2-3] stated that finger stiffness is programmable, and he investigated planar and spatial frictional grasping by replacing each finger with a virtual spring model and derived a grasp stiffness matrix. Funahashi et al. [4], Howard and Kumar [5], Lin et al. [6], and Shapiro et al. [7] explored the effect of local curvature at contact points. In these studies [1-7], frictionless sliding contact is represented by a one-dimensional linear spring model oriented along the initial contact normal, and frictional rolling contact is represented by a multidimensional linear translational spring model. Howard and Kumar [8] investigated enveloping grasping, but did not detail the analysis of the revolute joint stiffness model and frictionless sliding contact.

Yamada et al. [9-10] pointed out that the difference between frictionless sliding and frictional rolling

Manabu Yamada, professor, Ph.D., research fields: control system designs and their applications to robot systems.

Hidehiko Yamamoto, professor, Ph.D., research fields: production systems, intelligent systems, knowledge learning, and virtual manufacturing systems.

Corresponding author: Takayoshi Yamada, associate professor, Ph.D., research fields: grasping, manipulation, sensing, and automation systems. E-mail: yamat@gifu-u.ac.jp.

contacts is not spring dimension but contact condition. They used a multidimensional translational spring model not only for the rolling contact but also for sliding contact, and they clarified the physical status of the contact condition. This method admits the coexistence of frictionless sliding contact and frictional rolling contact during grasping. In Ref. [11], the contact surface geometry (metric tensor, curvature, and torsion) in the grasping of a single spatial object was investigated, while in Ref. [12], the grasping of multiple planar objects was explored. In Refs. [9-12], each finger is formulated with a multidimensional translational spring model, implying that each finger is constructed with prismatic joints, and its fingertip does not rotate in the workspace.

The human hand and the most developing mechanical hands are constructed with revolute joints, and each fingertip rotates in the workspace. Sarkar et al. [13], Maekawa et al. [14], Arimoto and Yoshida [15], Inoue and Hirai [16], and Nakashima and Hayakawa [17] investigated dynamic grasp stability including spring, mass, and damper effects. Harada et al. [18] discussed the manipulation of multiple objects. These studies included the finger structure; however, they only considered frictional rolling contact.

In Ref. [19], the static grasp stability of a single object was discussed where each finger is constructed with revolute joints. Based on Ref. [19], this paper refines formulations, provides properties of stiffness matrices, and adds distinctive numerical examples as follows. As both grasping with revolute joints and the frictionless sliding contact constraint are nonlinear conditions, grasp stability analysis has many difficulties and complexities. In this paper, we overcome these difficulties and provide our analysis procedure. First, we derive the contact constraints between each finger and a grasped object, including frictionless sliding contact and frictional rolling contact. The stiffness matrix of each finger is analytically derived by considering contact conditions. The effect of the local curvature at the contact point is discussed. The derived stiffness matrix of the revolute joint stiffness model is compared with that of the prismatic joint stiffness model [9]. The difference between the matrices of frictional rolling contact and frictionless sliding contact is shown. The gravity effect of the grasped object is also discussed. A grasp stiffness matrix is obtained from the sum of these effects. The effectiveness of our method is demonstrated through numerical examples. Grasp stability is evaluated by the eigenvalues of the grasp stiffness matrix, and the displacement motion direction is indicated by its corresponding eigenvectors. The joint angle effect is shown, and the coexistence case of frictional rolling and frictionless sliding contacts in grasping is also investigated.

The analysis of frictionless sliding contact is applicable for a case in which the contact friction condition is unknown prior to grasping. In this case, the optimum grasp location is determined from the grasp stability of the frictionless sliding contact model to make the grasp stable.

The paper is organized as follows: Section 2 shows problem formulation; section 3 provides fingertip position displacement; section 4 derives a stiffness matrix with frictionless sliding contact; section 5 derives a stiffness matrix with frictional rolling contact; section 6 obtains the difference of the matrices; section 7 explores gravity effect; section 8 obtains a stiffness matrix of a grasp; sections 9 and 10 provide numerical examples, and section 11 concludes this paper.

2. Problem Formulation

We assume that a single object is grasped by a multifingered hand (Fig. 1).

2.1 Assumptions

To clarify and simplify our problem, we analyze it under the following assumptions:

(A1) The object and the finger links are rigid bodies.

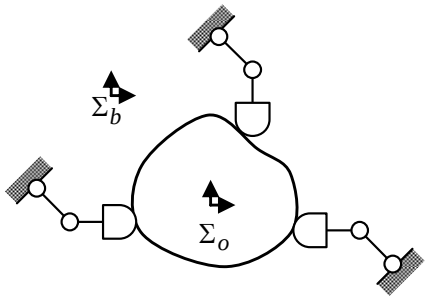

Fig. 1 Single object grasped by a multifingered hand with revolute joints.

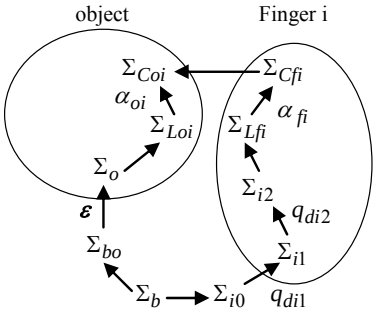

Fig. 2 Relation of coordinate frames.

(A2) There is a single-point contact between two bodies.

(A3) The initial grasp pose is given in a static (force and moment) equilibrium.

(A4) The local curvature at each contact point is given.

(A5) An infinitesimal pose (position and orientation) displacement of the object occurs because of external disturbance.

(A6) Each finger is constructed with two revolute joints. The relation between joint torque and joint angle displacement is replaced by a virtual revolute stiffness model.

(A7) In the case of frictionless contact, each finger slides on an object's surface. In the case of frictional contact, each finger rolls on the object's surface without slipping.

In Assumption (A6), the elasticity of each joint can be generated by an actual torsion spring for fixtures or by compliance control for robotic hands. To compare to the revolute joint model, the prismatic joint model is explained on the basis of Ref. [9]. The frictional case means that the contact force is within the contact friction, and the finger does not slide on the object's surface.

2.2 Nomenclature

We use the following coordinate frames (Fig. 2):

Σ_b : Base coordinate frame of the hand.

Σ_{i0} : Base coordinate frame of the *i*-th finger.

Σ_{ij} : Coordinate frame fixed in the *j*-th joint of the *i*-th finger.

Σ_{Lfi} : Contact coordinate frame fixed at the initial contact location on the *i*-th finger surface.

Σ_o : Object coordinate frame fixed in the object.

Σ_{Loi} : Contact coordinate frame fixed at the initial contact location on the object's surface.

A homogeneous transformation matrix of Σ_b in Σ_a is defined as follows:

$$ {}^{a}A_b = \left[\begin{array}{c|c} {}^{a}R_b & {}^{a}\boldsymbol{p}_b \\ \hline 0_{1\times 2} & 1 \end{array}\right] \in \mathbb{R}^{3\times 3} \tag{1} $$

where the vector ${}^{a}\boldsymbol{p}_b \in \mathbb{R}^2$ and the matrix ${}^{a}R_b \in \mathbb{R}^{2\times 2}$ denote the position and orientation, respectively.

2.3 Joint Angle and Joint Torque

Each finger is constructed with two revolute joints, and the angle of these joints is represented by

$$ \boldsymbol{q}_i = [q_{i1}, q_{i2}]^T \in \mathbb{R}^2 \tag{2} $$

The joint angle is decomposed into the following elements:

$$ q_{ij} = q_{nij} + q_{cij} + q_{dij} \tag{3} $$

where q_{nij} is the natural angle of the virtual joint spring, q_{cij} is the initial compression to generate the initial grasping force, and q_{dij} is the compression caused by the object pose displacement. The stiffness of the virtual spring is denoted by $S_i \in \mathbb{R}^{2\times 2}$, and the initial joint torque is given by

$$ \boldsymbol{\tau}_i = S_i \boldsymbol{q}_{ci} \in \mathbb{R}^2, \quad \boldsymbol{q}_{ci} = [q_{ci1}, q_{ci2}]^T \tag{4} $$

The angle displacement q_{dij} depends not only on the object displacement but also on the contact condition (frictionless sliding contact or frictional rolling contact). This relation is discussed in section 3.

3. Fingertip Position Displacement

3.1 Fingertip Displacement

A local coordinate frame on the finger at the initial contact point is given by

$$ {}^{b}A_{Lfi}(\boldsymbol{q}_i)={}^{b}A_{i0}\,{}^{i0}A_{i1}(q_{i1})\,{}^{i1}A_{i2}(q_{i2})\,{}^{i2}A_{Lfi} \tag{5}$$

For the revolute joints shown in Fig. 3,

$$ {}^{i,j-1}A_{ij}(q_{ij})={}^{i,j-1}A_{bij}(q_{nij}+q_{cij})A_{rot}(q_{dij}) \tag{6}$$

For the prismatic joint shown in Figs. 4-5,

$$ {}^{i,j-1}A_{ij}(q_{ij})={}^{i,j-1}A_{bij}(q_{nij}+q_{cij})A_{trans}(q_{dij}\boldsymbol{u}_1) \tag{7}$$

where

$$ A_{rot}(\theta)=\left[\begin{array}{c|c}\mathrm{Rot}(\theta) & 0_{2\times1}\\ \hline 0_{1\times2} & 1\end{array}\right],\quad \mathrm{Rot}(\theta)=\begin{bmatrix}\cos\theta & -\sin\theta\\ \sin\theta & \cos\theta\end{bmatrix}$$

$$ A_{trans}(\boldsymbol{x})=\left[\begin{array}{c|c}I_2 & \boldsymbol{x}\\ \hline 0_{1\times2} & 1\end{array}\right],\quad \boldsymbol{u}_1=\begin{bmatrix}1\\0\end{bmatrix},\quad \boldsymbol{u}_2=\begin{bmatrix}0\\1\end{bmatrix} \tag{8}$$

3.2 Object Displacement

A local coordinate frame on the object's surface at the initial contact point is given by

$$ {}^{b}A_{Loi}(\boldsymbol{\varepsilon})={}^{b}A_{bo}\,{}^{bo}A_{o}(\boldsymbol{\varepsilon})\,{}^{o}A_{Loi} \tag{9}$$

where frame Σ_{bo} is the initial configuration of Σ_o. The object pose displacement is represented by

$$ {}^{bo}A_{o}(\boldsymbol{\varepsilon})=A_{trans}(\boldsymbol{x})A_{rot}(\zeta),\quad {}^{bo}A_{o}(0)=I_3 \tag{10}$$

where $\boldsymbol{\varepsilon}=[\boldsymbol{x}^T,\zeta]\in\mathbb{R}^3$ is the object pose (position and orientation) displacement. The vector $\boldsymbol{x}\in\mathbb{R}^2$ and the scalar $\zeta\in\mathbb{R}$ are the translation and rotation, respectively.

3.3 Contact Constraint of Object and Each Finger

When the hand grasps the object, each fingertip is in contact with the object, and the following contact constraint is obtained (Figs. 6-7):

$$ {}^{b}A_{Lfi}(\boldsymbol{q}_i)\,{}^{Lfi}A_{Cfi}(\alpha_{fi})\,{}^{Cfi}A_{Coi}={}^{b}A_{Loi}(\boldsymbol{\varepsilon})\,{}^{Loi}A_{Coi}(\alpha_{oi}) \tag{11}$$

where

$$ {}^{Lfi}A_{Cfi}(\alpha_{fi})=\left[\begin{array}{c|c}\mathrm{Rot}(\kappa_{fi}\alpha_{fi}) & \{\mathrm{Rot}(\kappa_{fi}\alpha_{fi})-I_2\}\kappa_{fi}^{-1}\boldsymbol{u}_1\\ \hline 0_{1\times2} & 1\end{array}\right]$$

$$ ={}^{Lfi}A_{\kappa fi}A_{rot}(\kappa_{fi}\alpha_{fi})\,{}^{Lfi}A_{\kappa fi}^{-1}$$

$$ {}^{Loi}A_{Coi}(\alpha_{oi})={}^{Loi}A_{\kappa oi}A_{rot}(\kappa_{oi}\alpha_{oi})\,{}^{Loi}A_{\kappa oi}^{-1}$$

$$ {}^{Lfi}A_{\kappa fi}=A_{trans}(-\kappa_{fi}^{-1}\boldsymbol{u}_1),\quad {}^{Loi}A_{\kappa oi}=A_{trans}(-\kappa_{oi}^{-1}\boldsymbol{u}_1)$$

$$ {}^{Cfi}A_{Coi}=A_{rot}(\pi),\quad {}^{Lfi}A_{Cfi}(0)=I_3,\quad {}^{Loi}A_{Coi}(0)=I_3 \tag{12}$$

The parameters α_{fi} and α_{oi} are the arc lengths of the contact location displacement, κ_{fi} and κ_{oi} are

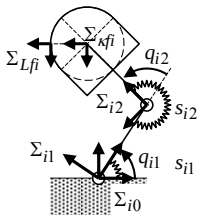

Fig. 3 Revolute joint stiffness model.

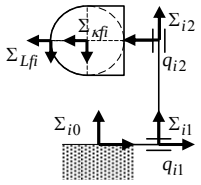

Fig. 4 Prismatic joint model.

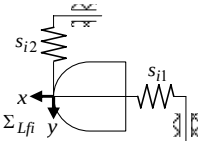

Fig. 5 Two-dimensional linear spring model.

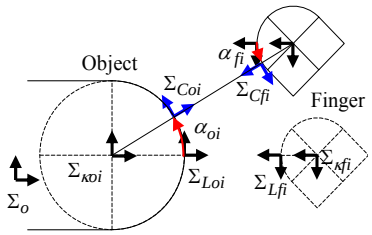

Fig. 6 Contact coordinate frames of object and finger.

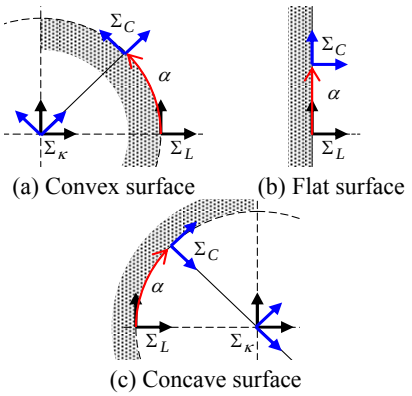

Fig. 7 Shape of body (finger or object) surface.

the local curvatures of the surfaces of the finger and object at the initial contact location, respectively. If the local shape is convex, flat, or concave, then the parameter κ is positive, zero, or negative, respectively. The matrix ${}^{L}A_{C}(\alpha)$ includes the flat surface case.

$$\lim_{\kappa\to 0} {}^{L}A_{C}(\alpha) = A_{trans}(\alpha \boldsymbol{u}_2) \tag{13}$$

From Assumption (A2), the local curvatures must satisfy $\kappa_{oi} + \kappa_{fi} > 0$. The frames $\Sigma_{\kappa fi}$ and $\Sigma_{\kappa oi}$ are given at the center of curvature of the surfaces of the finger and object, respectively. In Eq. (11), there are seven parameters.

The rotation component constraint of Eq. (11) is obtained by

$$\begin{aligned}&[I_2, 0_{2\times 1}]{}^{b}A_{Lfi}(\boldsymbol{q}_i)^{Lfi}A_{Cfi}(\alpha_{fi})^{Cfi}A_{Coi}\\ &\times\{{}^{b}A_{Loi}(\boldsymbol{\varepsilon})^{Loi}A_{Coi}(\alpha_{oi})\}^{-1}\begin{bmatrix} I_2 \\ 0_{1\times 2}\end{bmatrix} = I_2\end{aligned} \tag{14}$$

From Eq. (14), the following constraint is obtained:

$$\boldsymbol{c}_q^{T}\boldsymbol{q}_{di} - \zeta + \kappa_{fi}\alpha_{fi} - \kappa_{oi}\alpha_{oi} = 0 \tag{15}$$

with $\boldsymbol{c}_q^{T} = [1, 1]$ for the revolute joint and $\boldsymbol{c}_q^{T} = [0, 0]$ for the prismatic joint. In the revolute joint case, the derivation of the stiffness matrix is complicated because $\boldsymbol{c}_q$ is not zero.

4. Stiffness Matrix with Frictionless Sliding Contact

The joint angle displacement of each finger is replaced by the revolute stiffness model. When a grasped object is displaced by an external disturbance, each finger passively moves on the object's surface. The parameter α_{oi} depends not only on the object pose displacement $\boldsymbol{\varepsilon}$ but also on the contact friction condition. In this section, we derive this relation.

4.1 Joint Angle Displacement and Potential Energy

According to Eq. (15), one parameter can be reduced, and we select α_{fi} as a dependent parameter. To reduce the parameter, Eq. (11) is transformed into

$$\begin{aligned}&{}^{b}A_{Lfi}(\boldsymbol{q}_i)^{Lfi}A_{\kappa fi}A_{rot}(\kappa_{fi}\alpha_{fi})\\ &={}^{b}A_{Loi}(\boldsymbol{\varepsilon})^{Loi}A_{\kappa oi}A_{rot}(\kappa_{oi}\alpha_{oi})^{\kappa oi}A_{\kappa fi}\end{aligned} \tag{16}$$

Considering

$$A_{rot}(\theta)\begin{bmatrix} 0_{2\times 1} \\ 1\end{bmatrix} = \begin{bmatrix} 0_{2\times 1} \\ 1\end{bmatrix} \tag{17}$$

the position of $\Sigma_{\kappa fi}$ is obtained from

$$\begin{aligned}{}^{b}\boldsymbol{p}_{\kappa fi} &= [I_2, 0_{2\times 1}]{}^{b}A_{Lfi}(\boldsymbol{q}_i)^{Lfi}A_{\kappa fi}\begin{bmatrix} 0_{2\times 1} \\ 1\end{bmatrix}\\ &= [I_2, 0_{2\times 1}]{}^{b}A_{Loi}(\boldsymbol{\varepsilon})^{Loi}A_{\kappa oi}A_{rot}(\kappa_{oi}\alpha_{oi})^{\kappa oi}A_{\kappa fi}\begin{bmatrix} 0_{2\times 1} \\ 1\end{bmatrix}\end{aligned} \tag{18}$$

In Eq. (18), α_{fi} has been reduced. Eq. (18) can be written in the following implicit form:

$${}^{b}\boldsymbol{p}_{\kappa fi}(\boldsymbol{q}_{di}) = {}^{b}\boldsymbol{p}_{\kappa fi}(\boldsymbol{\varepsilon}, \alpha_{oi}) \tag{19}$$

Although Eq. (19) is a nonlinear constraint, if it is expressed explicitly,

$$\boldsymbol{q}_{di} = \boldsymbol{q}_{di}(\boldsymbol{\varepsilon}, \alpha_{oi}), \quad \boldsymbol{q}_{di}(0,0) = 0_{2\times 1} \tag{20}$$

the potential energy of each finger is given by

$$U_i(\boldsymbol{\varepsilon}, \alpha_{oi}) = \tfrac{1}{2}\{\boldsymbol{q}_{ci} + \boldsymbol{q}_{di}(\boldsymbol{\varepsilon}, \alpha_{oi})\}^{T} S_i \{\boldsymbol{q}_{ci} + \boldsymbol{q}_{di}(\boldsymbol{\varepsilon}, \alpha_{oi})\} \tag{21}$$

The first- and second-order partial derivatives are obtained as

$$\begin{bmatrix} U_{i,\varepsilon} \\ U_{i,\alpha}\end{bmatrix} = \begin{bmatrix} W_{\kappa fi} \\ -\kappa_{oi}{}^{\kappa fi}\boldsymbol{p}_{\kappa oi}\otimes {}^{\kappa fi}R_b\end{bmatrix}{}^{b}\boldsymbol{f}_{\kappa fi} \tag{22}$$

and

$$\begin{aligned}&\begin{bmatrix} U_{i,\varepsilon\varepsilon} & U_{i,\alpha\varepsilon} \\ U_{i,\varepsilon\alpha} & U_{i,\alpha\alpha}\end{bmatrix}\\ &= \left\{\begin{bmatrix} W_{\kappa fi} \\ -\kappa_{oi}{}^{\kappa fi}\boldsymbol{p}_{\kappa oi}\otimes {}^{\kappa fi}R_b\end{bmatrix}{}^{b}J_{\kappa fi}^{-T}\right\}\{S_i - S_{\kappa fi}\}\\ &\times\left\{\begin{bmatrix} W_{\kappa fi} \\ -\kappa_{oi}{}^{\kappa fi}\boldsymbol{p}_{\kappa oi}\otimes {}^{\kappa fi}R_b\end{bmatrix}{}^{b}J_{\kappa fi}^{-T}\right\}^{T}\\ &-{}^{b}\boldsymbol{f}_{\kappa fi}^{T}{}^{b}R_o{}^{o}\boldsymbol{p}_{\kappa fi}\begin{bmatrix}\boldsymbol{v}_\zeta \\ 0\end{bmatrix}\begin{bmatrix}\boldsymbol{v}_\zeta \\ 0\end{bmatrix}^{T}\\ &+{}^{b}\boldsymbol{f}_{\kappa fi}^{T}{}^{b}R_{\kappa fi}{}^{\kappa fi}\boldsymbol{p}_{\kappa oi}\left[\begin{array}{c|c} 0_{3\times 3} & \kappa_{oi}\boldsymbol{v}_\zeta \\ \hline \kappa_{oi}\boldsymbol{v}_\zeta^{T} & \kappa_{oi}^{2}\end{array}\right]\end{aligned} \tag{23}$$

where $U_{i,\varepsilon}$ is the first-order partial derivative of U_i by the variable $\boldsymbol{\varepsilon}$, $U_{i,\alpha\varepsilon}$ is the partial derivative of $U_{i,\varepsilon}$ by the variable α_{oi} (see Appendix A), and the symbol $\otimes$ denotes the cross product. The following symbols are also used.

$$\begin{aligned}&W_{\kappa fi} = \frac{\partial^{b}\boldsymbol{p}_{\kappa fi}^{T}(\boldsymbol{\varepsilon}, \alpha_{oi})}{\partial \boldsymbol{\varepsilon}}\Big|_0 = \begin{bmatrix} I_2 \\ {}^{o}\boldsymbol{p}_{\kappa fi}\otimes\end{bmatrix}{}^{o}R_b\\ &{}^{b}\boldsymbol{f}_{\kappa fi} = {}^{b}J_{\kappa fi}^{-T}\boldsymbol{\tau}_i, \quad \boldsymbol{v}_\zeta = [0,0,1]^{T}, \quad \Omega = \mathrm{Rot}(\pi/2)\end{aligned} \tag{24}$$

For the revolute joint case,

$$
\begin{aligned}
{}^{b}J_{\kappa fi} &= \frac{\partial {}^{b}\boldsymbol{p}_{\kappa fi}(\boldsymbol{q}_{di})}{\partial \boldsymbol{q}_{di}^{T}}|_{0} = [{}^{b}R_{i1}\Omega^{i1}\boldsymbol{p}_{\kappa fi}, {}^{b}R_{i2}\Omega^{i2}\boldsymbol{p}_{\kappa fi}] \\
S_{\kappa fi} &= \frac{\partial^{2}\{{}^{b}\boldsymbol{f}_{\kappa fi}^{T}\,{}^{b}\boldsymbol{p}_{\kappa fi}(\boldsymbol{q}_{di})\}}{\partial \boldsymbol{q}_{di}\partial \boldsymbol{q}_{di}^{T}}|_{0} \\
&= -{}^{b}\boldsymbol{f}_{\kappa fi}^{T}\,{}^{b}R_{i1}\,{}^{i1}\boldsymbol{p}_{\kappa fi}\begin{bmatrix}1 & 0\\ 0 & 0\end{bmatrix} - {}^{b}\boldsymbol{f}_{\kappa fi}^{T}\,{}^{b}R_{i2}\,{}^{i2}\boldsymbol{p}_{\kappa fi}\begin{bmatrix}0 & 1\\ 1 & 1\end{bmatrix}
\end{aligned} \tag{25}
$$

For the prismatic joint case,

$${}^{b}J_{\kappa fi} = [{}^{b}R_{i1}\boldsymbol{u}_{1}, {}^{b}R_{i2}\boldsymbol{u}_{1}] = -{}^{b}R_{\kappa fi}, \quad S_{\kappa fi} = 0_{2\times 2} \tag{26}$$

4.2 Frictionless Sliding Contact

In the case of frictionless contact, each finger slides on the object's surface, and its potential energy will be the local minimum (Fig. 8). Hence, we have

$$\frac{\partial U_{i}(\boldsymbol{\varepsilon}, \alpha_{oi})}{\partial \alpha_{oi}} = 0 \tag{27}$$

and

$$\frac{\partial^{2} U_{i}(\boldsymbol{\varepsilon}, \alpha_{oi})}{\partial \alpha_{oi}^{2}} > 0 \tag{28}$$

Although the implicit form (27) is nonlinear on $\boldsymbol{\varepsilon}$ and α_{oi}, if the displacement length α_{oi} is explicitly expressed by

$$\alpha_{oi} = \alpha_{oi}^{fs}(\boldsymbol{\varepsilon}) \tag{29}$$

the potential energy with a sliding contact is given by

$$U_{i}^{fs}(\boldsymbol{\varepsilon}) = U_{i}(\boldsymbol{\varepsilon}, \alpha_{oi}^{fs}(\boldsymbol{\varepsilon})) \tag{30}$$

where the right superscript "fs" denotes the frictionless sliding contact. Note that Eq. (30) is nonlinear, but we need not solve it explicitly. From Eq. (30), the wrench vector (i.e., force and moment vectors) and the stiffness matrix of the sliding contact finger are respectively calculated by

$$G_{i}^{fs} = \frac{\partial U_{i}^{fs}(\boldsymbol{\varepsilon})}{\partial \boldsymbol{\varepsilon}}|_{0} = W_{\kappa fi}\,{}^{b}\boldsymbol{f}_{\kappa fi} \tag{31}$$

and

$$H_{i}^{fs} = \frac{\partial^{2} U_{i}^{fs}(\boldsymbol{\varepsilon})}{\partial \boldsymbol{\varepsilon}\partial \boldsymbol{\varepsilon}^{T}}|_{0} = U_{i,\varepsilon\varepsilon} - U_{i,\alpha\varepsilon}U_{i,\alpha\alpha}^{-1}U_{i,\varepsilon\alpha} \tag{32}$$

The detailed derivation procedure of Eqs. (31)-(32) is described in Appendices B and C. According to Eq. (32), it is clear that the matrix H_{i}^{fs} especially depends on the configuration of $\Sigma_{\kappa fi}$.

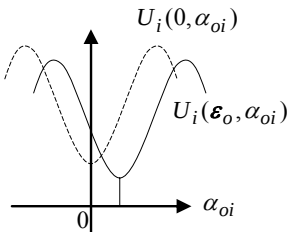

Fig. 8 Potential energy condition for frictionless sliding contact.

Before grasp stability is evaluated using Eq. (32), we must check the stability of each finger (28), i.e., $U_{i,\alpha\alpha} > 0$. If the joint stiffness S_{i} and the joint torque $\boldsymbol{\tau}_{i}$ are assigned the wrong values, this condition is not satisfied.

Comparing the stiffness matrices with the revolute joint (25) and the prismatic joint (26), the following relation is obtained:

$${}^{b}J_{\kappa fi}^{-T}\{S_{i} - S_{\kappa fi}\}{}^{b}J_{\kappa fi}^{-1} = {}^{b}R_{\kappa fi}\{S_{pi}^{fs}\}^{\kappa fi}R_{b} \tag{33}$$

where S_{pi}^{fs} means prismatic stiffness at the frame $\Sigma_{\kappa fi}$ to distinguish the revolute stiffness S_{i}, as shown in Fig. 9a. When S_{i} is given, the resultant stiffness at $\Sigma_{\kappa fi}$ is calculated by

$$S_{pi}^{fs} = {}^{\kappa fi}R_{b}\,{}^{b}J_{\kappa fi}^{-T}\{S_{i} - S_{\kappa fi}\}{}^{b}J_{\kappa fi}^{-1}{}^{b}R_{\kappa fi} \tag{34}$$

According to Eq. (34), S_{pi}^{fs} depends not only on ${}^{b}J_{\kappa fi}$ and S_{i} but also on the joint torque $\boldsymbol{\tau}_{i}$ in $S_{\kappa fi}$. When S_{pi}^{fs} is given as a design parameter in a reverse way, the revolute stiffness must be controlled at

$$S_{i} = \{{}^{b}J_{\kappa fi}^{T}\,{}^{b}R_{\kappa fi}\}S_{pi}^{fs}\{{}^{b}J_{\kappa fi}^{T}\,{}^{b}R_{\kappa fi}\}^{T} + S_{\kappa fi} \tag{35}$$

According to Eq. (35), S_{i} must include not only S_{pi}^{fs} but also $S_{\kappa fi}$.

4.3 Property of Sliding Contact Stiffness Matrix

We discuss the properties of Eqs. (31)-(32). From Appendix D, the effect of local curvatures is obtained as

$$
\begin{aligned}
\frac{\partial G_{i}^{fs}}{\partial \kappa_{oi}} &= \frac{\partial G_{i}^{fs}}{\partial \kappa_{fi}} = 0_{3\times 1} \\
\frac{\partial H_{i}^{fs}}{\partial \kappa_{oi}} &= \{{}^{b}\boldsymbol{f}_{\kappa fi}^{T}\,{}^{b}R_{\kappa fi}\boldsymbol{u}_{1}\}Q_{i}^{fs}\{Q_{i}^{fs}\}^{T} \\
\frac{\partial H_{i}^{fs}}{\partial \kappa_{fi}} &= \{{}^{b}\boldsymbol{f}_{\kappa fi}^{T}\,{}^{b}R_{\kappa fi}\boldsymbol{u}_{1}\}\boldsymbol{b}_{i}^{fs}\{\boldsymbol{b}_{i}^{fs}\}^{T}
\end{aligned} \tag{36}
$$

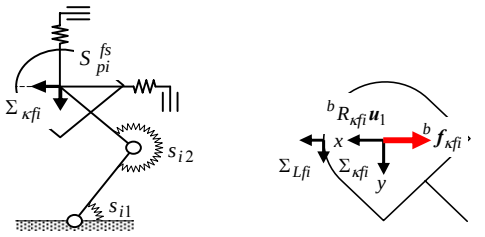

(a) Stiffness relation (b) Compression force

Fig. 9 Sliding contact case.

where

$$
\begin{aligned}
Q_i^{fs} &= -U_{i,\alpha\varepsilon}U_{i,\alpha\alpha}^{-1} \\
\boldsymbol{b}_i^{fs} &= -\kappa_{fi}^{-1}\{\boldsymbol{v}_\zeta + \kappa_{oi}Q_i^{fs}\} \\
&\quad + \kappa_{fi}^{-1}\{W_{\kappa fi} - \kappa_{oi}Q_i^{fs}[{}^{\kappa fi}\boldsymbol{p}_{\kappa oi}\otimes]^{\kappa fi}R_b\}{}^b J_{\kappa fi}^{-T}\boldsymbol{c}_q
\end{aligned}
\tag{37}
$$

Because the torque $\boldsymbol{\tau}_i$ is generated by the spring compression as shown in Eq. (4), and the relationship between $\boldsymbol{\tau}_i$ and ${}^b\boldsymbol{f}_{\kappa fi}$ is given by Eq. (24), the vector ${}^b\boldsymbol{f}_{\kappa fi}$ is an applied force at $\Sigma_{\kappa fi}$ from the grasped object as shown in Fig. 9b. The force ${}^b\boldsymbol{f}_{\kappa fi}$ is an inward vector to the finger's surface, but the vector ${}^bR_{\kappa fi}\boldsymbol{u}_1$ is an outward vector. Consequently, the coefficient ${}^b\boldsymbol{f}_{\kappa fi}^T{}^bR_{\kappa fi}\boldsymbol{u}_1$ is a negative value, and Eq. (36) is negative semi-definite. Therefore, grasp stability is increased when the local curvature κ_{oi} or κ_{fi} is decreased. It has been theoretically shown that the stability of Fig. 10b is higher than that of Fig. 10a. The local curvature change (error) affects the stability in the Q_i^{fs} and $\boldsymbol{b}_i^{fs}$ directions. It is clarified that the directions vary from not only the finger pose but also the contact force.

5. Stiffness Matrix with Frictional Rolling Contact

In the case of frictional contact (Fig. 11), each finger rolls on the object's surface, and the following rolling contact constraint is obtained:

$$\alpha_{oi} + \alpha_{fi} = 0 \tag{38}$$

From Eqs. (15) and (38), the following explicit form is obtained:

$$\boldsymbol{\alpha}_i^{fr}(\boldsymbol{\varepsilon},\boldsymbol{q}_{di}) = \begin{bmatrix}\alpha_{oi}^{fr}(\boldsymbol{\varepsilon},\boldsymbol{q}_{di}) \\ \alpha_{fi}^{fr}(\boldsymbol{\varepsilon},\boldsymbol{q}_{di})\end{bmatrix} = \frac{\boldsymbol{c}_q^T\boldsymbol{q}_{di} - \boldsymbol{v}_\zeta^T\boldsymbol{\varepsilon}}{\kappa_{oi}+\kappa_{fi}}\begin{bmatrix}1 \\ -1\end{bmatrix} \tag{39}$$

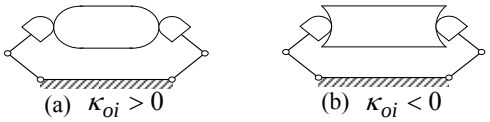

(a) $\kappa_{oi} > 0$ (b) $\kappa_{oi} < 0$

Fig. 10 Difference in the local curvature at the contact point.

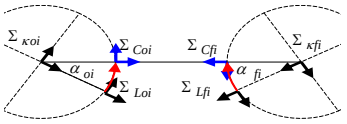

Fig. 11 Contact location displacement for a rolling contact case.

where the right superscript "fr" denotes the frictional rolling contact. In the case of rolling contact, the frame Σ_{Lfi} is suitable for the calculation of the stiffness matrix. The position of Σ_{Lfi} is obtained from Eq. (11).

$$
\begin{aligned}
{}^b\boldsymbol{p}_{Lfi} &= [I_2, 0_{2\times1}]{}^bA_{Lfi}(\boldsymbol{q}_i)\begin{bmatrix}0_{2\times1} \\ 1\end{bmatrix} \\
&= [I_2, 0_{2\times1}]{}^bA_{Loi}(\boldsymbol{\varepsilon})^{Loi}A_{Coi}(\alpha_{oi}) \\
&\quad \times {}^{Cfi}A_{Coi}^{-1}{}^{Lfi}A_{Cfi}^{-1}(\alpha_{fi})\begin{bmatrix}0_{2\times1} \\ 1\end{bmatrix}
\end{aligned}
\tag{40}
$$

From Eqs. (39)-(40), the following implicit form is obtained:

$${}^b\boldsymbol{p}_{Lfi}(\boldsymbol{q}_{di}) = {}^b\boldsymbol{p}_{Lfi}(\boldsymbol{\varepsilon}, \boldsymbol{\alpha}_i^{fr}(\boldsymbol{\varepsilon},\boldsymbol{q}_{di})) \tag{41}$$

Eq. (41) is nonlinear on $\boldsymbol{\varepsilon}$ and $\boldsymbol{q}_{di}$, but it can be formally represented explicitly by the joint angle displacement:

$$\boldsymbol{q}_{di} = \boldsymbol{q}_{di}^{fr}(\boldsymbol{\varepsilon}) \tag{42}$$

Note that Eq. (42) is nonlinear, but we do not need to solve it explicitly. The potential energy of each finger is given by

$$U_i^{fr}(\boldsymbol{\varepsilon}) = \tfrac{1}{2}\{\boldsymbol{q}_{ci} + \boldsymbol{q}_{di}^{fr}(\boldsymbol{\varepsilon})\}^T S_i\{\boldsymbol{q}_{ci} + \boldsymbol{q}_{di}^{fr}(\boldsymbol{\varepsilon})\} \tag{43}$$

From Eq. (43), the stiffness matrix of the rolling contact finger is given by

$$G_i^{fr} = \frac{\partial U_i^{fr}(\boldsymbol{\varepsilon})}{\partial\boldsymbol{\varepsilon}}|_0 = W_{Lfi}{}^b\boldsymbol{f}_{Lfi} \tag{44}$$

and

$$
\begin{aligned}
H_i^{fr} &= \frac{\partial^2 U_i^{fr}(\boldsymbol{\varepsilon})}{\partial\boldsymbol{\varepsilon}\partial\boldsymbol{\varepsilon}^T}|_0 \\
&= \{W_{Lfi}{}^bJ_{Lfi}^{-T}\}\{S_i - S_{Lfi}\}\{W_{Lfi}{}^bJ_{Lfi}^{-T}\}^T \\
&\quad -\{{}^b\boldsymbol{f}_{Lfi}^T{}^bR_o{}^o\boldsymbol{p}_{Lfi}\}\boldsymbol{v}_\zeta\boldsymbol{v}_\zeta^T \\
&\quad -\frac{{}^b\boldsymbol{f}_{Lfi}^T{}^bR_{Lfi}\boldsymbol{u}_1}{\kappa_{oi}+\kappa_{fi}}\{W_{Lfi}{}^bJ_{Lfi}^{-T}\boldsymbol{c}_q - \boldsymbol{v}_\zeta\} \\
&\quad \times\{W_{Lfi}{}^bJ_{Lfi}^{-T}\boldsymbol{c}_q - \boldsymbol{v}_\zeta\}^T
\end{aligned}
\tag{45}
$$

where

$$W_{Lfi}=\frac{\partial^b \boldsymbol{p}_{Lfi}^T(\boldsymbol{\varepsilon},\boldsymbol{\alpha}_i)}{\partial \boldsymbol{\varepsilon}}|_0=\begin{bmatrix} I_2 \\ {}^o\boldsymbol{p}_{Lfi}\otimes \end{bmatrix}{}^oR_b$$

$${}^b\boldsymbol{f}_{Lfi}={}^bJ_{Lfi}^{-T}\boldsymbol{\tau}_i \tag{46}$$

For the revolute joint case,

$${}^bJ_{Lfi}=\frac{\partial^b \boldsymbol{p}_{Lfi}(\boldsymbol{q}_{di})}{\partial \boldsymbol{q}_{di}^T}|_0=[{}^bR_{i1}\Omega^{i1}\boldsymbol{p}_{Lfi},{}^bR_{i2}\Omega^{i2}\boldsymbol{p}_{Lfi}]$$

$$\begin{aligned} S_{Lfi}&=\frac{\partial\{{}^b\boldsymbol{p}_{Lfi}^T(\boldsymbol{q}_{di}){}^b\boldsymbol{f}_{Lfi}\}}{\partial \boldsymbol{q}_{di}\partial \boldsymbol{q}_{di}^T}|_0 \\ &=-{}^b\boldsymbol{f}_{Lfi}^T{}^bR_{i1}{}^{i1}\boldsymbol{p}_{Lfi}\begin{bmatrix}1&0\\0&0\end{bmatrix}-{}^b\boldsymbol{f}_{Lfi}^T{}^bR_{i2}{}^{i2}\boldsymbol{p}_{Lfi}\begin{bmatrix}0&1\\1&1\end{bmatrix}\end{aligned} \tag{47}$$

For the prismatic joint case,

$${}^bJ_{Lfi}=[{}^bR_{i1}\boldsymbol{u}_1,{}^bR_{i2}\boldsymbol{u}_1]=-{}^bR_{Lfi},\quad S_{Lfi}=0_{2\times 2} \tag{48}$$

The detailed derivations of Eqs. (44)-(45) are explained in Appendix E. According to the above equations, we have clarified that the matrix H_i^{fr} depends in particular on the configuration of Σ_{Lfi}.

In a manner similar to the sliding contact case Eq. (35), even if the revolute joint stiffness is controlled at

$$S_i=\{{}^bJ_{Lfi}^T{}^bR_{Lfi}\}S_{pi}^{fr}\{{}^bJ_{Lfi}^T{}^bR_{Lfi}\}^T+S_{Lfi} \tag{49}$$

where S_{pi}^{fr} is the prismatic stiffness at Σ_{Lfi} (Fig. 12a), the difference in the stiffness matrices between the revolute joint and the prismatic joint appears according to Appendix F.

$$\begin{aligned} H_{di}^{fr}&=\frac{{}^b\boldsymbol{f}_{Lfi}^T{}^bR_{Lfi}\boldsymbol{u}_1}{\kappa_{oi}+\kappa_{fi}} \\ &\times[\{W_{Lfi}{}^bJ_{Lfi}^{-T}\boldsymbol{c}_q-\boldsymbol{v}_\zeta\}\{W_{Lfi}{}^bJ_{Lfi}^{-T}\boldsymbol{c}_q-\boldsymbol{v}_\zeta\}^T-\boldsymbol{v}_\zeta\boldsymbol{v}_\zeta^T]\end{aligned} \tag{50}$$

This difference results from finger rotation because $\boldsymbol{c}_q$ is not zero in the case of a revolute joint.

The effects of local curvatures κ_{oi} and κ_{fi} are given as

$$\frac{\partial G_i^{fr}}{\partial \kappa_{oi}}=\frac{\partial G_i^{fr}}{\partial \kappa_{fi}}=0_{3\times 1} \tag{51}$$

$$\frac{\partial H_i^{fr}}{\partial \kappa_{oi}}=\frac{\partial H_i^{fr}}{\partial \kappa_{fi}}=\{{}^b\boldsymbol{f}_{Lfi}^T{}^bR_{Lfi}\boldsymbol{u}_1\}Q_i^{fr}\{Q_i^{fr}\}^T \tag{52}$$

where

$$Q_i^{fr}=\frac{\partial \alpha_{oi}^{fr}(\boldsymbol{\varepsilon},\boldsymbol{q}_{di}^{fr}(\boldsymbol{\varepsilon}))}{\partial \boldsymbol{\varepsilon}}|_0=\frac{W_{Lfi}{}^bJ_{Lfi}^{-T}\boldsymbol{c}_q-\boldsymbol{v}_\zeta}{\kappa_{oi}+\kappa_{fi}} \tag{53}$$

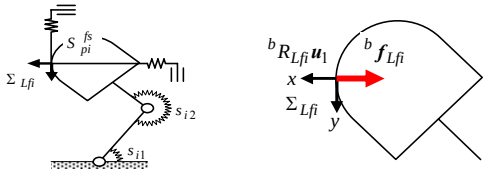

(a) Stiffness relation (b) Compression force

Fig. 12 A rolling contact case.

The vector ${}^b\boldsymbol{f}_{Lfi}$ is the compression force represented at Σ_{Lfi}, as shown in Fig. 12b. Because the coefficient ${}^b\boldsymbol{f}_{Lfi}^T{}^bR_{Lfi}\boldsymbol{u}_1$ is negative, Eq. (52) is negative semi-definite. Therefore, it has been theoretically shown that grasp stability is increased when the object or finger local curvature is decreased. The local curvature change affects the stability in the Q_i^{fr} direction, and it does not vary on the contact force, as shown in Eq. (53). In the case of the prismatic joints ($\boldsymbol{c}_q^T=[0,0]$), the curvature change affects only the rotational stability.

6. Difference of Stiffness Matrices with Frictionless Sliding Contact and Frictional Rolling Contact

To compare the stiffness matrices of frictionless sliding and frictional rolling contacts, we assume that the contact force generates along the normal direction at the contact point ($U_{i,\alpha}=0$). From Appendix G, the difference in the stiffness matrices H_i^{fs} and H_i^{fr} is obtained as

$$H_i^{fd}=H_i^{fr}-H_i^{fs}=U_{i,\alpha\alpha}Q_i^{fd}\{Q_i^{fd}\}^T \tag{54}$$

where

$$Q_i^{fd}=Q_i^{fr}-Q_i^{fs} \tag{55}$$

As we have $U_{i,\alpha\alpha}>0$ from Eq. (28), the difference H_i^{fd} is positive semi-definite. Hence, the grasp stability of frictional rolling contact is higher than that of a frictionless sliding contact. The contact friction condition affects the stability in the Q_i^{fd} direction.

As a result, if the contact friction condition is unknown prior to grasping, grasp parameters should be designed on the basis of frictionless sliding contact to obtain a stable grasp. After this is done, the designed grasp becomes stable.

7. Gravity Effect

The gravity effect for an object of mass m is calculated by the potential energy of the object. This energy is calculated by

$$U_g(\boldsymbol{\varepsilon}) = \{{}^b\boldsymbol{p}_g(\boldsymbol{\varepsilon}) - {}^b\boldsymbol{p}_g(0)\}^T \{m\,{}^b\boldsymbol{g}\} \tag{56}$$

where

$${}^b\boldsymbol{p}_g(\boldsymbol{\varepsilon}) = [I_2, 0_{2\times 1}]\,{}^bA_{bo}\,{}^{bo}A_o(\boldsymbol{\varepsilon})\,{}^oA_g \begin{bmatrix} 0_{2\times 1} \\ 1 \end{bmatrix} \tag{57}$$

The matrix ${}^oA_g$ represents the configuration of the object's center-of-gravity frame with respect to Σ_o. The vector ${}^b\boldsymbol{g}$ is the gravity acceleration in the frame Σ_b. From Eqs. (56)-(57), the first- and second-order partial derivatives are respectively obtained as follows:

$$G_g = \frac{\partial U_g(\boldsymbol{\varepsilon})}{\partial \boldsymbol{\varepsilon}}|_0 = \begin{bmatrix} I_2 \\ {}^o\boldsymbol{p}_g \otimes \end{bmatrix} {}^oR_b \{m\,{}^b\boldsymbol{g}\} \tag{58}$$

$$H_g = \frac{\partial^2 U_g(\boldsymbol{\varepsilon})}{\partial \boldsymbol{\varepsilon} \partial \boldsymbol{\varepsilon}^T}|_0 = -\{{}^o\boldsymbol{p}_g^T\}\,{}^oR_b\{m\,{}^b\boldsymbol{g}\}\boldsymbol{v}_\zeta \boldsymbol{v}_\zeta^T \tag{59}$$

8. Stiffness Matrix of Grasp

The total potential energy of the grasp is the sum of each potential energy:

$$U(\boldsymbol{\varepsilon}) = \sum_{i=1}^{n} U_i^{fc}(\boldsymbol{\varepsilon}) + U_g(\boldsymbol{\varepsilon}). \tag{60}$$

The first-order partial derivative of Eq. (60) is given by

$$G = \sum_{i=1}^{n} G_i^{fc} + G_g \tag{61}$$

The grasp stiffness matrix is obtained from the sum of each stiffness matrix:

$$H = \sum_{i=1}^{n} H_i^{fc} + H_g \tag{62}$$

The grasp stability is evaluated using the eigenvalues of Eq. (62) when Eq. (61) is zero (static equilibrium). If all eigenvalues are positive, the grasp is stable. The corresponding eigenvectors indicate the displacement motion direction of the grasp.

For the case of finger with both prismatic and revolute joints, $\boldsymbol{c}_q$, ${}^bJ_{\kappa fi}$, $S_{\kappa fi}$, ${}^bJ_{Lfi}$, and S_{Lfi} are provided in Appendix H.

9. Numerical Example 1

To demonstrate the effectiveness of our analysis, numerical examples are presented below. In this paper, the number of objects is limited to a single object, but the number of fingers is unlimited. To verify that the result of our analysis coincides with human intuition, simple examples are shown in Fig. 13. In this example, the gravity effect is neglected.

9.1 Numerical Setting

A single object is grasped by two fingers with revolute joints. Each link length is 0.03 m. The radius of the local curvature of the fingertip is $\kappa_{fi}^{-1} = 0.005\,\mathrm{m}$. The radius of the local curvature of the object is $\kappa_{oi}^{-1} = 0.01\,\mathrm{m}$. The initial joint angle is given by

$$q_{11} = \pi/4\,,\quad q_{12} = \pi/2$$
$$q_{21} = 3\pi/4\,,\ \text{and}\ \ q_{22} = -\pi/2 \tag{63}$$

The joint stiffness is given by

$$S_i = \mathrm{diag}[1, 1]\ \mathrm{N\cdot m/rad} \tag{64}$$

The initial contact force is given by

$${}^b\boldsymbol{f}_{Lf1} = [f_x, 0]^T\,,\quad {}^b\boldsymbol{f}_{Lf2} = [-f_x, 0]^T \tag{65}$$

These forces are applied from the object to the fingers, and the red arrows shown in Fig. 13 are these counterforces. From the above settings, the following grasp stiffness matrix is obtained:

$$H = \begin{bmatrix} h_{xx} & 0 & h_{\zeta x} \\ 0 & h_{yy} & 0 \\ h_{x\zeta} & 0 & h_{\zeta\zeta} \end{bmatrix} \tag{66}$$

The eigenvalues of Eq. (66) are calculated by

$$\lambda_1 = h_{yy}$$
$$\left.\begin{matrix} \lambda_2 \\ \lambda_3 \end{matrix}\right\} = \frac{1}{2}\left\{ h_{xx} + h_{\zeta\zeta} \pm \sqrt{(h_{xx} - h_{\zeta\zeta})^2 + 4h_{x\zeta}h_{\zeta x}} \right\} \tag{67}$$

9.2 Frictionless Sliding Contact Case

In a frictionless sliding contact case, the grasp is intuitively unstable. We show that a similar result is obtained by our method. The elements of Eq. (66) are given as

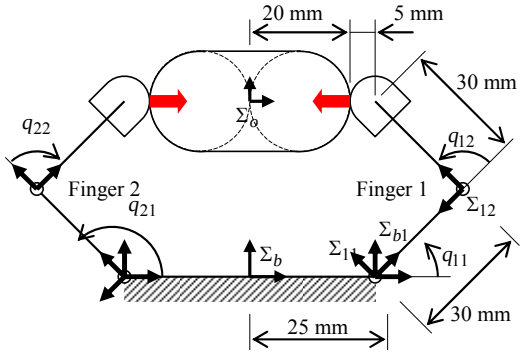

Fig. 13 Single object grasped by two-fingered hand with revolute joints.

$$h_{xx}=\frac{50\{20000-300(2+\sqrt{2})f_x-9f_x^2\}}{9(125-3f_x)}$$

$$h_{yy}=\frac{-50000f_x}{3(125-3f_x)},\quad h_{\zeta\zeta}=\frac{-(625-9f_x)f_x}{150(125-3f_x)}$$

$$h_{x\zeta}=h_{\zeta x}=\frac{(100+3\sqrt{2}f_x)f_x}{3(125-3f_x)} \tag{68}$$

As shown in Eq. (68), the advantage of our method is that we are able to derive analytical equations.

We have $U_{i,\alpha\alpha}=50(125-3f_x)$. Hence, if $f_x<125/3$ N, the stability condition of each finger (28) is satisfied. The eigenvalues are shown in Fig. 14. The eigenvalues and eigenvectors are listed in Table 1 for a case in which the contact force is $f_x=3$ N. The eigenvectors represent the object pose displacement. Displacements corresponding to these three eigenvectors are shown in Fig. 15. The dotted line represents the initial grasping pose, and the solid line represents the displaced pose. The direction is exaggerated for easy understanding, because our analysis assumes an infinitesimal displacement from Assumption (A5). In Fig. 15a, the object moves upward (downward), and then the fingers generate an upward (downward) force and push the object away. Hence, this mode is unstable. In Fig. 15b, the object mainly moves in the x direction, and the fingers generate the force and moment restoring the object pose to the initial pose. Hence, this mode is stable. In Fig. 15c, the object mainly rotates in the counterclockwise (clockwise) direction, and then the fingers generate an overturning wrench. Hence, this mode is unstable.

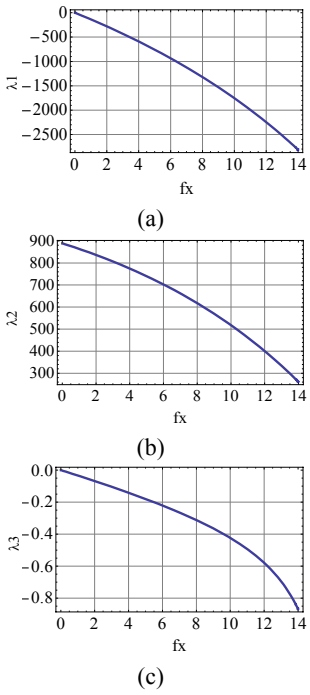

Fig. 14. Eigenvalues of a frictionless sliding contact case.

Table 1 Eigenvalues and eigenvectors of sliding contact case with 3 N.

	Eigenvalue	Eigenvector
(a)	−431.034	0, 1, 0
(b)	806.812	0.9999, 0, 0.0012
(c)	−0.104274	−0.0012, 0, 0.9999

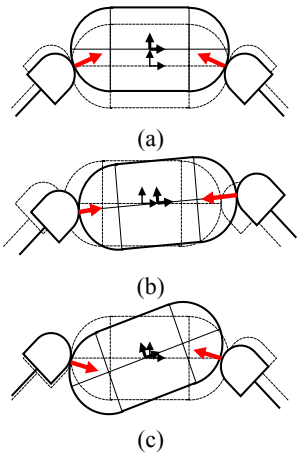

Fig. 15 Motion of eigenvectors of frictionless sliding contact case.

Because these three motions are mixed owing to various external disturbances in actual practice, this grasp is unstable. As human beings have experienced (a) and (c), they can intuitively judge this grasp to be unstable.

From the above description, the grasp stability and its displacement motion direction are evaluated by the eigenvalues and eigenvectors of the grasp stiffness matrix.

From Eq. (34), the resultant stiffness of each finger at $\Sigma_{\kappa fi}$ is given by

$$\left.\begin{matrix} S_{p1}^{fs} \\ S_{p2}^{fs} \end{matrix}\right\} = \frac{50}{9}\begin{bmatrix} 100 & \mp(100-3\sqrt{2}f_x) \\ \mp(100-3\sqrt{2}f_x) & 500 \end{bmatrix} \quad (69)$$

This means that the primary axes of the matrix (69) are rotated from the normal direction at the contact point. Hence, the interference terms $(h_{x\zeta}, h_{\zeta x})$ become nonzero.

In the case of the prismatic joint shown in Fig. 16, if the prismatic stiffness is given by

$$S_{pi}^{fs} = \mathrm{diag}[s_x, s_y] \quad (70)$$

the grasp stiffness matrix is obtained as the following diagonal matrix:

$$H = \mathrm{diag}\left[2s_x,\ -\frac{400 s_y f_x}{3s_y - 200 f_x},\ -\frac{(s_y - 40 f_x) f_x}{10(3s_y - 200 f_x)}\right] \quad (71)$$

From Eq. (35), a revolute joint stiffness generating Eq. (70) is given by

$$S_i = \frac{1}{20000}\begin{bmatrix} 36s_x & 6(3s_x + 50\sqrt{2} f_x) \\ 6(3s_x + 50\sqrt{2} f_x) & 3\{3(s_x + s_y) + 100\sqrt{2} f_x\} \end{bmatrix} \quad (72)$$

As shown in Eq. (72), the contact force must be included for controlling stiffness.

9.3 Frictional Rolling Contact Case

In the case of frictional rolling contact, the elements of Eq. (66) are given by

$$\begin{aligned} h_{xx} &= 200\frac{400(658+99\sqrt{2}) + 3(706-47\sqrt{2}) f_x}{45369} \\ h_{yy} &= 400\frac{(73-12\sqrt{2})(3000-f_x)}{15123} \\ h_{\zeta\zeta} &= \frac{24000(73-12\sqrt{2}) + (-26357+3504\sqrt{2}) f_x}{756150} \\ h_{x\zeta} &= h_{\zeta x} = 4\frac{-600(122+49\sqrt{2}) + (209-2106\sqrt{2}) f_x}{15123} \end{aligned} \quad (73)$$

The eigenvalues of Eq. (73) are shown in Fig. 17. The eigenvalues and eigenvectors with $f_x = 3$ N are listed in Table 2.

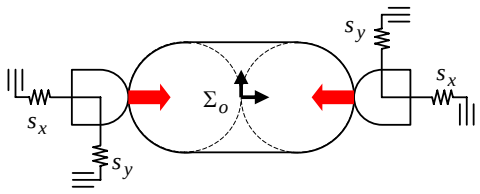

Fig. 16 Single object grasped by two-fingered hand with a linear spring model.

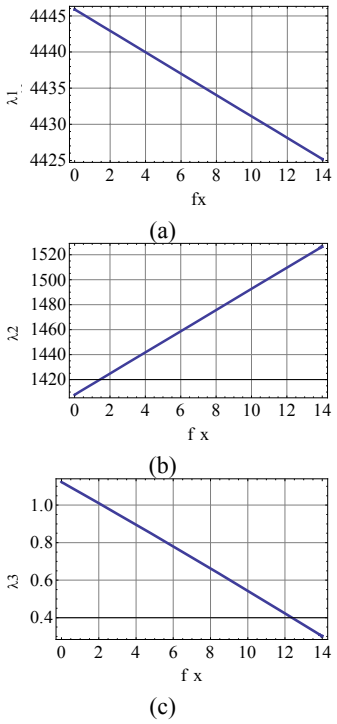

Fig. 17 Eigenvalues of a frictional rolling contact case.

The displacements corresponding to three eigenvectors are shown in Fig. 18. In Fig. 18a, the object moves upward (downward), and then the fingers generate a resultant downward (upward) force. Hence, this mode is stable. In Fig. 18b, the object mainly moves in the x direction, and the finger generates the force and moment restoring the object pose to the initial pose. Hence, this mode is stable. In Fig. 18c, the object mainly rotates in the counterclockwise (clockwise) direction, and then the fingertip forces generate the moment overturning the object pose, while the joint spring stiffness generates the moment restoring the pose. When $f_x > 18.8$ N, the overturning moment exceeds the restoring moment. Hence, the stability of this mode depends upon the initial finger force.

Table 2 Eigenvalues and eigenvectors of a rolling contact case with 3 N.

	Eigenvalue	Eigenvector
(a)	4441.45	0, 1, 0
(b)	1433.25	−0.9997, 0, 0.0227
(c)	0.9531	0.0227, 0, 0.9997

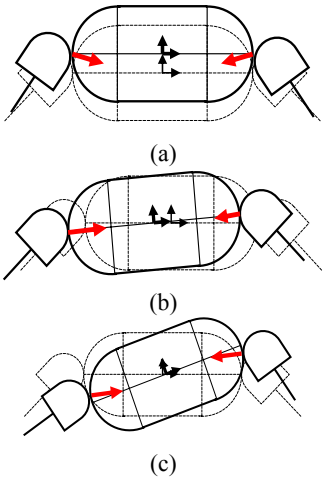

Fig. 18 Motion of eigenvectors of a frictional rolling contact case.

When the grasping force is large, the grasp becomes unstable. This phenomenon occurs in a type of grasping an object such as being picked up with chopsticks.

As the joint stiffness becomes greater, the grasp stability is increased. Hence, to stabilize the grasp—even if the object is grasped using a large contact force ($f_x > 18.8$ N)—the joint stiffness K_i must be increased. For this reason, to generate a stable grasp, it is thought that human beings adjust (increase) the joint stiffness when grasping an object using a large contact force. In contrast, robot hands can change the contact force applied independently against the joint stiffness by using computer control.

From Eq. (55), we have

$$\left.\begin{matrix} Q_1^{fd} \\ Q_2^{fd} \end{matrix}\right\} = \frac{\begin{bmatrix} -25\{200(11+5\sqrt{2})+(4+47\sqrt{2})f_x\} \\ \pm 100\{250(12-\sqrt{2})-(1-6\sqrt{2})f_x\} \\ 500(12-\sqrt{2})-(73-12\sqrt{2})f_x \end{bmatrix}}{3550(125-3f_x)} \tag{74}$$

The perpendicular direction to Q_1^{fd} and Q_2^{fd} is given by

$$\boldsymbol{\varepsilon}^{fd} = \begin{bmatrix} 500(12-\sqrt{2})-(73-12\sqrt{2})f_x \\ 0 \\ 25\{200(11+5\sqrt{2})+(4+47\sqrt{2})f_x\} \end{bmatrix} \tag{75}$$

In this direction, the grasp stability with rolling contact is equivalent to that with sliding contact. The difference value in this direction is calculated as

$$\{\boldsymbol{\varepsilon}^{fd}\}^T\{H_1^{fd}+H_2^{fd}\}\boldsymbol{\varepsilon}^{fd}=0 \tag{76}$$

When the prismatic stiffness shown in Fig. 16 is given by

$$S_{pi}^{fr} = \mathrm{diag}[s_x, s_y] \tag{77}$$

the grasp stiffness matrix becomes

$$H = \mathrm{diag}\left[2s_x,\quad 2s_y,\quad \frac{3s_y-125f_x}{3750}\right] \tag{78}$$

Note that the matrix (78) is invariable, even if the location of the origin of the prismatic stiffness changes, because fingertip rotation is not considered in this model. From Eq. (49), the revolute joint stiffness generating Eq. (77) is given by

$$S_i = \frac{1}{40000}\begin{bmatrix} 72s_x+s_y+200f_x \\ 36s_x+(1+3\sqrt{2})(s_y+200f_x) \\ 36s_x+(1+3\sqrt{2})(s_y+200f_x) \\ 18s_x+(19+6\sqrt{2})s_y+200(1+3\sqrt{2})f_x \end{bmatrix} \tag{79}$$

In this case, the grasp stiffness matrix becomes

$$H = \mathrm{diag}\left[2s_x,\quad 2s_y,\quad \frac{3s_y-125f_x}{3750}\right] + \frac{f_x(-73+12\sqrt{2})}{378075} \times \begin{bmatrix} 20000 & 0 & 100(5+6\sqrt{2}) \\ 0 & 20000 & 0 \\ 100(5+6\sqrt{2}) & 0 & 12(1+2\sqrt{2}) \end{bmatrix} \tag{80}$$

The second term of Eq. (80) is obtained from Eq. (50) and results from finger rotation.

9.4 Curvature Effect

The matrix elements of the sliding contact with $f_x = 3$ N are

$$h_{xx} = -25\frac{200(-19919+900\sqrt{2})+(-14519+900\sqrt{2})\kappa_o}{9(12500+49\kappa_o)}$$

$$h_{yy} = \frac{-75000\kappa_o}{12500+49\kappa_o},\quad h_{\zeta\zeta} = \frac{897(50-\kappa_o)}{25(12500+49\kappa_o)}$$

$$h_{x\zeta}=h_{\zeta x}=\frac{-3(100+9\sqrt{2})(50-\kappa_o)}{12500+49\kappa_o} \tag{81}$$

The eigenvalues are shown in Fig. 19. All the eigenvalues decrease with the increasing curvature value, as proved in Eq. (36). According to Eq. (36), the curvature change (error) has an effect in the following directions:

$$\left.\begin{matrix}Q_1^{fs}\\ Q_2^{fs}\end{matrix}\right\}=\frac{1}{12500+49\kappa_o}\begin{bmatrix}25(100+9\sqrt{2})\\ \mp 12500\\ -299\end{bmatrix} \tag{82}$$

The perpendicular direction to these vectors is given by

$$\boldsymbol{\varepsilon}^{fs}=[299,\quad 0,\quad 25(100+9\sqrt{2})]^T \tag{83}$$

The grasp stability in this direction is independent of the change in the local curvature of the object. The value is calculated as

$$\{\boldsymbol{\varepsilon}^{fs}\}^T H\boldsymbol{\varepsilon}^{fs}=37375\{18839-900\sqrt{2}\}/9 \tag{84}$$

and is independent of the local curvature of the object. The direction $\boldsymbol{b}_i^{fs}$ is given by

$$\left.\begin{matrix}\boldsymbol{b}_1^{fs}\\ \boldsymbol{b}_2^{fs}\end{matrix}\right\}=\frac{\begin{bmatrix}-25\{200(3+100\sqrt{2})+(203+100\sqrt{2})\kappa_o\}\\ \pm 50(500+9\sqrt{2})\kappa_o\\ -(500+9\sqrt{2})(50-\kappa_o)\end{bmatrix}}{400(12500+49\kappa_o)} \tag{85}$$

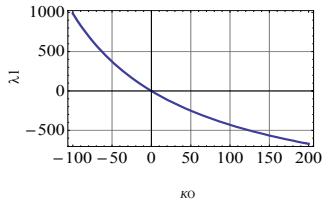

(a)

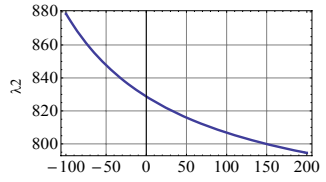

(b)

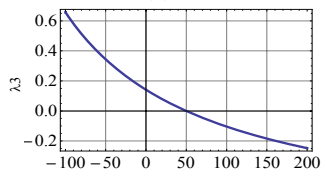

(c)

Fig. 19 Curvature effect on sliding contact grasp.

The perpendicular direction to these vectors is given by

$$\begin{bmatrix}(500+9\sqrt{2})(50-\kappa_o)\\ 0\\ -25\{200(3+100\sqrt{2})+(203+100\sqrt{2})\kappa_o\}\end{bmatrix} \tag{86}$$

The grasp stability in this direction is independent of the change in the local curvature of the finger.

The matrix elements of rolling contact are

$$\begin{aligned}h_{xx}&=520000\frac{20836+2997\sqrt{2}}{45369(200+\kappa_o)}\\ &\quad+200\frac{266926+39609\sqrt{2}}{45369(200+\kappa_o)}\kappa_o\\ h_{yy}&=\frac{-400(-73+12\sqrt{2})(200000+997\kappa_o)}{5041(200+\kappa_o)}\\ h_{\zeta\zeta}&=2\frac{1120927-181776\sqrt{2}}{5041(200+\kappa_o)}\\ &\quad+\frac{276001-47856\sqrt{2}}{126025(200+\kappa_o)}\kappa_o\\ h_{x\zeta}&=h_{\zeta x}\\ &=-400\frac{48161+23434\sqrt{2}}{5041(200+\kappa_o)}\\ &\quad-16\frac{6103+3071\sqrt{2}}{5041(200+\kappa_o)}\kappa_o\end{aligned} \tag{87}$$

The eigenvalues are shown in Fig. 20. All the eigenvalues decrease with an increase in the value of curvature as proved in Eq. (52). The curvature change affects the following displacement direction:

$$\left.\begin{matrix}Q_1^{fr}\\ Q_2^{fr}\end{matrix}\right\}=\frac{1}{71(200+\kappa_o)}\begin{bmatrix}200(1-6\sqrt{2})\\ \pm 200(1-6\sqrt{2})\\ -(67+24\sqrt{2})\end{bmatrix} \tag{88}$$

The perpendicular direction to these vectors is given by

$$\boldsymbol{\varepsilon}^{fr}=[67+24\sqrt{2},\quad 0,\quad 200(1-6\sqrt{2})]^T \tag{89}$$

The rolling contact grasp stability in this direction is independent of the object and the change in the local curvature of the finger. The value is given as

$$\{\boldsymbol{\varepsilon}^{fr}\}^T H\boldsymbol{\varepsilon}^{fr}=1000\{172622+57597\sqrt{2}\}/9 \tag{90}$$

and it is independent of the local curvature.

9.5 Joint Angle Effect

We investigate the effect of joint angle, as shown in Fig. 21. The joint angle is assigned as

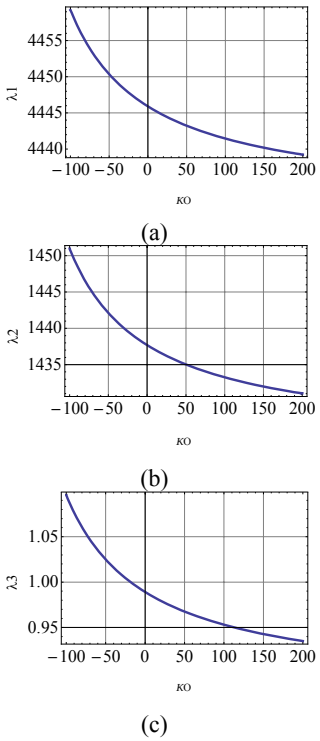

Fig. 20 Curvature effect on rolling contact grasp.

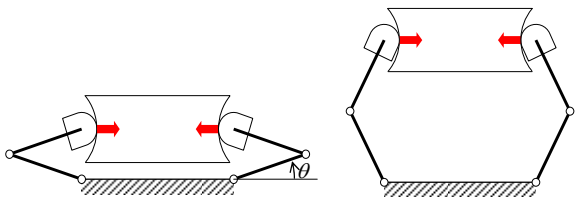

(a) Small case of angle θ (b) Large case of angle θ

Fig. 21 Difference in joint angle.

$$q_{11} = \theta, \quad q_{12} = \pi - 2\theta$$
$$q_{21} = \pi - \theta, \quad q_{22} = 2\theta - \pi \tag{91}$$

The object's local curvature is assigned as $\kappa_{oi} = -50\ \mathrm{m}^{-1}$. The force is fixed at $f_x = 3\ \mathrm{N}$. The other settings are the same as those of IX.A.

In the case of frictionless sliding contact, we have

$$h_{xx} = \frac{25\,(21719 - 1800\cos\theta - 1719\cos 2\theta)}{9(134 + 9\cos 2\theta)\sin^2\theta}$$
$$h_{yy} = \frac{50000}{134 + 9\cos 2\theta}, \quad h_{\zeta\zeta} = \frac{2(598 - 27\cos 2\theta)}{25(134 + 9\cos 2\theta)}$$
$$h_{x\zeta} = h_{\zeta x} = \frac{-8(50 + 9\cos\theta)}{(134 + 9\cos 2\theta)\tan\theta} \tag{92}$$

The eigenvalues are shown in Fig. 22. The corresponding eigenvectors of Figs. 22a-22c are in a strictly y-directional translation, mainly x-directional translation, and mainly rotation, respectively. When the joint angle θ is larger, the horizontal stability is smaller, the vertical stability is higher, and the rotational stability is higher.

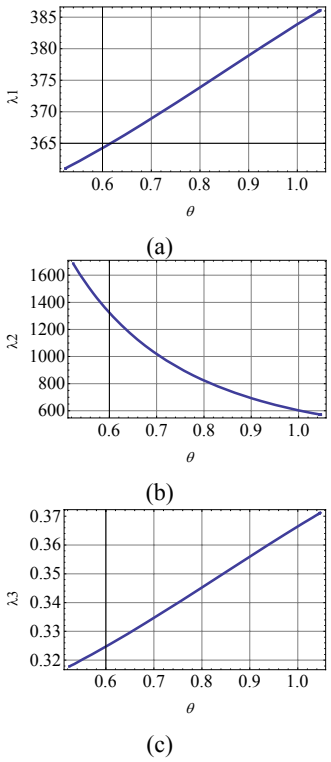

Fig. 22 Eigenvalues of joint angle effect on sliding contact grasp.

In the case of the frictional rolling contact, we have

$$h_{xx} = \frac{200\,(2063 + 1209\cos\theta + 1863\cos 2\theta)}{9(1 + 12\cos\theta)^2\sin^2\theta}$$
$$h_{yy} = \frac{400400}{(1 + 12\cos\theta)^2}$$
$$h_{\zeta\zeta} = \frac{2(1933 + 24\cos\theta - 72\cos 2\theta)}{25(1 + 12\cos\theta)^2}$$
$$h_{x\zeta} = h_{\zeta x} = \frac{-8(112 + 201\cos\theta + 12\cos 2\theta)}{(1 + 12\cos\theta)^2\sin\theta} \tag{93}$$

The eigenvalues are shown in Fig. 23. The directions of the corresponding eigenvalues are similar to those of the sliding contact case. The effect of the joint angle is also similar to that in the sliding contact case.

These results coincide with the experience of human beings. To select an optimum grasp pose from the joint angle shown in Figs. 22-23, the following method is feasible. First, the units of the parameters

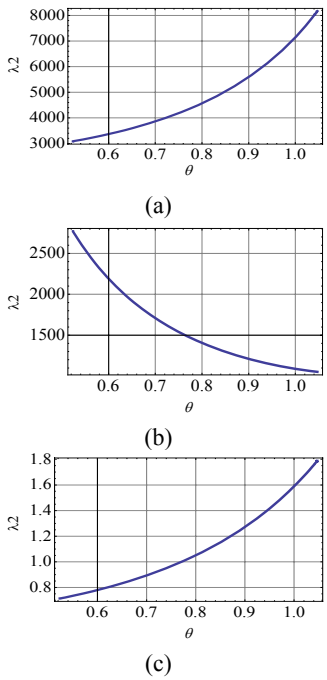

Fig. 23 Eigenvalues of joint angle effect to the rolling contact grasp.

are normalized according to grasping tasks. In this example, the units [m] and [rad] are used as the translational and rotational object displacements, respectively. If units [mm] and [deg] are required to normalize the units, a weighting matrix can be used for the stiffness matrix. Second, the eigenvalues and eigenvectors of the normalized grasp stiffness matrix are derived, where the number of the positive eigenvalues is invariable even if the units are normalized. Finally, an optimum grasp is selected using a suitable index based on the eigenvalues and eigenvectors. For example, the index selects the grasp maximizing the lowest eigenvalue.

10. Numerical Example 2

Our analysis allows the coexistence of frictionless sliding contacts and frictional rolling contacts in a grasp. We investigate the grasp shown in Fig. 24. An object is grasped by four fingers. Fingers 1 and 4 denote frictionless sliding contact, and fingers 2 and 3 denote frictional rolling contact. The surface curvature and the link length of each finger are similar to those in Example 1.

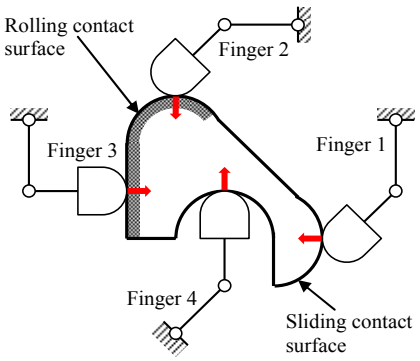

Fig. 24 Object grasped by four fingers.

Table 3 Eigenvalues and eigenvectors of Eq. (98).

	Eigenvalue	Eigenvector
(a)	10383.3	0.7432, 0.6690, −0.0134
(b)	4399.25	−0.6690, 0.7432, 0.0003
(c)	1.7208	0.0102, 0.0088, 0.9999

$$q_{11}=\pi/2,\ q_{12}=-\pi/4,\ q_{21}=\pi/2,\ q_{22}=\pi/4$$
$$q_{31}=\pi/2,\ q_{32}=\pi/2,\ q_{41}=\pi/2,\ q_{22}=\pi/4 \quad (94)$$

The local curvatures of the object's surface are assigned as

$$\kappa_{o1}^{-1}=\kappa_{o2}^{-1}=0.01\ \text{mm}$$
$$\kappa_{O3}=0,\ \kappa_{o4}^{-1}=-0.01\ \text{m} \quad (95)$$

The configuration of Σ_{Loi} with respect to Σ_b is assigned as

$${}^b\boldsymbol{p}_{Lo1}=[0.02,-0.01]^T,\ {}^bR_{Lo1}=\text{Rot}(0)$$
$${}^b\boldsymbol{p}_{Lo2}=[-0.01,0.02]^T,\ {}^bR_{Lo2}=\text{Rot}(\pi/2)$$
$${}^b\boldsymbol{p}_{Lo3}=[-0.02,0]^T,\ {}^bR_{Lo3}=\text{Rot}(-\pi)$$
$${}^b\boldsymbol{p}_{Lo4}=[0,0]^T,\ {}^bR_{Lo4}=\text{Rot}(-\pi/2) \quad (96)$$

Each finger pushes perpendicular to the object's surface, and the fingertip force is assigned as

$${}^b\boldsymbol{f}_{Lf1}=[f,0]^T,\ {}^b\boldsymbol{f}_{Lf2}=[0,f]^T$$
$${}^b\boldsymbol{f}_{Lf3}=[-f,0]^T,\ {}^b\boldsymbol{f}_{Lf4}=[0,-f]^T \quad (97)$$

From these settings and f =3 N, the following grasp stiffness matrix is obtained:

$$H=\begin{bmatrix} 7703.73 & 2974.62 & -104.332 \\ 2974.62 & 7076.95 & -92.3923 \\ -104.332 & -92.3923 & 3.59208 \end{bmatrix} \quad (98)$$

The eigenvalues and eigenvectors are listed in Table 3. There are no unstable modes.

As shown in the above examples, our proposed method can evaluate grasp stability—including the effects of revolute joint—contact condition.

11. Conclusions

This paper analyzed grasp stability from the viewpoint of a potential energy method. The contributions made by this paper are (1) The effect of a revolute joint model was investigated. (2) Stiffness matrices were derived by considering not only frictional rolling contact but also frictionless sliding contact. It was shown that rolling contact grasp stability is more stable than sliding contact grasp stability by deriving the difference between these two matrices. The grasp displacement direction affected by the contact condition was obtained. In the case of frictionless sliding contact, the stable condition for each finger was provided. (3) The stiffness matrix of the revolute joint model was compared with that of the prismatic one, and then the relation between the revolute joint model and the prismatic one was provided. In the case of frictionless sliding contact, it was shown that the property of the prismatic joint stiffness can be generated by the revolute joint stiffness, where the generated stiffness is affected by not only the revolute joint stiffness but also the joint torque. In the case of frictional rolling contact, the difference between the grasp stiffness matrices of the revolute joint stiffness model and the prismatic one was derived. (4) The effect of the local curvature was shown analytically by deriving the partial derivatives of the matrices. The grasp displacement direction affected by the local curvature change was also obtained. (5) The gravity effect of the grasped object was also discussed. (6) The grasp stiffness matrix was also derived analytically. It was shown that the coexistence of frictional rolling and frictionless sliding contacts in a single grasp is possible. (7) The effectiveness of our method was demonstrated through numerical examples. The grasp stability and its corresponding motion direction were evaluated by the eigenvalues and eigenvectors of the matrix.

This method is applicable to grasp position planning for robotic hands and the planning of fixture positions for manufacturing systems.

For a future study, the grasping of multiple objects will be analyzed. We will also investigate a case where the number of joints is redundant and spatial objects are grasped. In these cases, there are many difficulties. For example, in a spatial grasp, the number of displacement parameters is significantly increased, the constraint of Eq. (15) is much complicated, and the sliding contact constraint (27) and the rolling contact constraint (38) are also much complicated.

In this paper, we did not consider a case where the tangential component of each finger force exceeds the contact friction condition, and finger sliding occurs in rolling contact. In our future study, we will investigate this complicated case.

Acknowledgment

The authors thank Shu-ichi Yamanaka, Naoki Mizuno and Tatsushi Ooba for their useful comments. This work was supported in part by a Grant-in-Aid for Scientific Research (C) (No. 23560285).

References

[1] H. Hanafusa, H. Asada, Stable prehension by a robot hand with elastic fingers, Robot Motion Planning and Control MIT Press, 1982, pp. 323-335.

[2] V.D. Nguyen, The synthesis of stable grasps in the plane, in: Proc. of IEEE Int. Conf. on Robotics and Automation (ICRA), 1986, pp. 884-889.

[3] V.D. Nguyen, Constructing stable grasps, Int. J. of Robotics Research 7 (3) (1988) 3-16.

[4] Y. Funahashi, T. Yamada, M. Tate, Y. Suzuki, Grasp stability analysis considering the curvatures at contact points, in: Proc. of IEEE ICRA, 1996, pp. 3040-3046.

[5] W. Howard, V. Kumar, On the stability of grasped objects, IEEE Trans. on Robotics and Automation 12 (6) (1996) 904-917.

[6] Q. Lin, J. Burdick, E. Rimon, Computation and analysis of natural compliance in fixturing and grasping arrangements, IEEE Trans. on Robotics 20 (4) (2004) 651-667.

[7] A. Shapiro, E. Rimon, S. Shoval, On the passive force closure set of planar grasps and fixtures, Int. J. of Robotics Research 29 (11) (2010) 1435-1454.
[8] W.S. Howard, V. Kumar, Modeling and analysis of the compliance and stability of enveloping grasps, in: Proc. of IEEE ICRA, 1995, pp. 1367-1372.
[9] T. Yamada, S. K. Saha, N. Mimura, Y. Funahashi, Stability analysis of planar grasps with 2D-virtual spring model, J. of Robotics and Mechatronics 11 (4) (1999) 274-282.
[10] T. Yamada, T. Koishikura, Y. Mizuno, N. Mimura, Y. Funahashi, Stability analysis of 3D grasps by a multifingered hand (in Japanese), Trans. of JSME C 69 (670) (2003) 127-134.
[11] T. Yamada, T. Taki, M. Yamada, Y. Funahashi, H. Yamamoto, Static stability analysis of spatial grasps including contact surface geometry, Advanced Robotics 25 (3) (2011) 447-472.
[12] T. Yamada, S. Yamanaka, M. Yamada, Y. Funahashi, H. Yamamoto, Static stability analysis of grasping multiple objects in 2D, Int. J. of Information Acquisition 7 (2) (2010) 119-134.
[13] N. Sarkar, X. Yun, V. Kumar, Dynamic control of 3-D rolling contacts in two-arm manipulation, IEEE Trans. on Robotics and Automation 13 (3) (1997) 364-376.
[14] H. Maekawa, K. Taine, K. Komoriya, Kinematics, Statics and stiffness effect of a 3D grasp by multifingered hand with rolling contact at the fingertip (in Japanese), J. of RSJ 16 (2) (1998) 205-213.
[15] S. Arimoto, M. Yoshida, Modeling and control of three-dimensional grasping by a pair of robot fingers, SICE J. Control, Measurement, and System Integration 1 (1) (2008) 2-11.
[16] T. Inoue, S. Hirai, Parallel-distributed model of soft fingertips in three-dimensional grasping and manipulation, in: Proc. 2008 IEEE Int. Conf. on Robotics and Biomimetics, 2009, pp. 895-902.
[17] A. Nakashima, Y. Hayakawa, Stability analysis of grasped object by soft-fingers with 3-dimensional deformation based on moment stability, in: Proc. of IEEE Int. Conf. on Decision and Control, 2009, pp. 8192-8199.
[18] K. Harada, M. Kaneko, T. Tsuji, Rolling based manipulation for multiple objects, in: Proc. IEEE ICRA, 2000, pp. 3888-3895.
[19] T. Yamada, M. Yamada, H. Yamamoto, Stability analysis of a single object grasped by a multifingered hand with angular joints in 2D, in: Proc of IEEE Int. Conf. on Mechatronics and Automation, 2011, pp. 1457-1464.

Appendix A: Partial Derivatives

The first-order partial derivatives of the homogeneous transformation matrices used in this paper are obtained as

$$\frac{\partial A_{trans}(\boldsymbol{x})}{\partial x} = \frac{\partial A_{trans}(\boldsymbol{x})}{\partial x} A_{trans}^{-1}(\boldsymbol{x}) A_{trans}(\boldsymbol{x}) = \left[\begin{array}{c|c} 0_{2\times 2} & \boldsymbol{u}_1 \\ \hline 0_{1\times 2} & 0 \end{array}\right] A_{trans}(\boldsymbol{x})$$

$$\frac{\partial A_{rot}(\zeta)}{\partial \zeta} = A_{rot}(\zeta) A_{rot}^{-1}(\zeta) \frac{\partial A_{rot}(\zeta)}{\partial \zeta} = A_{rot}(\zeta) \left[\begin{array}{c|c} \Omega & 0_{2\times 1} \\ \hline 0_{1\times 2} & 0 \end{array}\right]$$

$$\frac{\partial {}^{Loi}A_{Coi}(\alpha_{oi})}{\partial \alpha_{oi}} = \kappa_{oi}\, {}^{Loi}A_{\kappa oi} \left[\begin{array}{c|c} \Omega & 0_{2\times 1} \\ \hline 0_{1\times 2} & 0 \end{array}\right] {}^{Loi}A_{\kappa oi}^{-1}\, {}^{Loi}A_{Coi}(\alpha_{oi}) \tag{99}$$

For the revolute joint case,

$$\frac{\partial {}^{i,j-1}A_{ij}(q_{ij})}{\partial q_{dij}} = {}^{i,j-1}A_{ij}(q_{ij}) \left[\begin{array}{c|c} \Omega & 0_{2\times 1} \\ \hline 0_{1\times 2} & 0 \end{array}\right] \tag{100}$$

For the prismatic joint case,

$$\frac{\partial {}^{i,j-1}A_{ij}(q_{ij})}{\partial q_{dij}} = {}^{i,j-1}A_{ij}(q_{ij}) \left[\begin{array}{c|c} 0_{2\times 2} & \boldsymbol{u}_1 \\ \hline 0_{1\times 2} & 0 \end{array}\right] \tag{101}$$

The second-order partial derivatives are obtained in a similar manner. The first- and second-order partial derivatives of Eq. (16) and other factors are given as follows:

$$
{}^{a}A_{b}\left[\begin{array}{c|c}\Omega_b & \boldsymbol{v}_b \\ \hline 0_{1\times 2} & 0\end{array}\right]{}^{b}A_{c}=\left[\begin{array}{c|c}{}^{a}R_b\Omega_b{}^{b}R_c & {}^{a}R_b\boldsymbol{v}_b+{}^{a}R_b\Omega_b{}^{b}\boldsymbol{p}_c \\ \hline 0_{1\times 2} & 0\end{array}\right]
$$

$$
{}^{a}A_{b}\left[\begin{array}{c|c}\Omega_b & \boldsymbol{v}_b \\ \hline 0_{1\times 2} & 0\end{array}\right]{}^{b}A_{c}\left[\begin{array}{c|c}\Omega_c & \boldsymbol{v}_c \\ \hline 0_{1\times 2} & 0\end{array}\right]{}^{c}A_{d}=\left[\begin{array}{c|c}{}^{a}R_b\Omega_b{}^{b}R_c\Omega_c{}^{c}R_d & {}^{a}R_b\Omega_b{}^{b}R_c\{\boldsymbol{v}_c+\Omega_c{}^{c}\boldsymbol{p}_d\} \\ \hline 0_{1\times 2} & 0\end{array}\right] \tag{102}
$$

The first- and second-order partial derivatives of Eq. (21) are given by

$$
\begin{bmatrix}U_{i,\varepsilon}\\ U_{i,\alpha}\end{bmatrix}=\begin{bmatrix}\dfrac{\partial U_i(\boldsymbol{\varepsilon},\alpha_{oi})}{\partial \boldsymbol{\varepsilon}}|_0\\ \dfrac{\partial U_i(\boldsymbol{\varepsilon},\alpha_{oi})}{\partial \alpha_{oi}}|_0\end{bmatrix}=\begin{bmatrix}\dfrac{\partial \boldsymbol{q}_{di}^{T}(\boldsymbol{\varepsilon},\alpha_{oi})}{\partial \boldsymbol{\varepsilon}}|_0\\ \dfrac{\partial \boldsymbol{q}_{di}^{T}(\boldsymbol{\varepsilon},\alpha_{oi})}{\partial \alpha_{oi}}|_0\end{bmatrix}\boldsymbol{\tau}_i
$$

$$
\begin{aligned}
\begin{bmatrix}U_{i,\varepsilon\varepsilon} & U_{i,\alpha\varepsilon}\\ U_{i,\varepsilon\alpha} & U_{i,\alpha\alpha}\end{bmatrix}&=\begin{bmatrix}\dfrac{\partial^2 U_i(\boldsymbol{\varepsilon},\alpha_{oi})}{\partial \boldsymbol{\varepsilon}\partial \boldsymbol{\varepsilon}^{T}}|_0 & \dfrac{\partial^2 U_i(\boldsymbol{\varepsilon},\alpha_{oi})}{\partial \boldsymbol{\varepsilon}\partial \alpha_{oi}}|_0\\ \dfrac{\partial^2 U_i(\boldsymbol{\varepsilon},\alpha_{oi})}{\partial \alpha_{oi}\partial \boldsymbol{\varepsilon}^{T}}|_0 & \dfrac{\partial^2 U_i(\boldsymbol{\varepsilon},\alpha_{oi})}{\partial \alpha_{oi}\partial \alpha_{oi}}|_0\end{bmatrix}\\
&=\begin{bmatrix}\dfrac{\partial \boldsymbol{q}_{di}^{T}(\boldsymbol{\varepsilon},\alpha_{oi})}{\partial \boldsymbol{\varepsilon}}|_0\\ \dfrac{\partial \boldsymbol{q}_{di}^{T}(\boldsymbol{\varepsilon},\alpha_{oi})}{\partial \alpha_{oi}}|_0\end{bmatrix}S_i\begin{bmatrix}\dfrac{\partial \boldsymbol{q}_{di}^{T}(\boldsymbol{\varepsilon},\alpha_{oi})}{\partial \boldsymbol{\varepsilon}}|_0\\ \dfrac{\partial \boldsymbol{q}_{di}^{T}(\boldsymbol{\varepsilon},\alpha_{oi})}{\partial \alpha_{oi}}|_0\end{bmatrix}^{T}+\begin{bmatrix}\dfrac{\partial^2\{\boldsymbol{\tau}_i^{T}\boldsymbol{q}_{di}(\boldsymbol{\varepsilon},\alpha_{oi})\}}{\partial \boldsymbol{\varepsilon}\partial \boldsymbol{\varepsilon}^{T}}|_0 & \dfrac{\partial^2\{\boldsymbol{\tau}_i^{T}\boldsymbol{q}_{di}(\boldsymbol{\varepsilon},\alpha_{oi})\}}{\partial \boldsymbol{\varepsilon}\partial \alpha_{oi}}|_0\\ \dfrac{\partial^2\{\boldsymbol{\tau}_i^{T}\boldsymbol{q}_{di}(\boldsymbol{\varepsilon},\alpha_{oi})\}}{\partial \alpha_{oi}\partial \boldsymbol{\varepsilon}^{T}}|_0 & \dfrac{\partial^2\{\boldsymbol{\tau}_i^{T}\boldsymbol{q}_{di}(\boldsymbol{\varepsilon},\alpha_{oi})\}}{\partial \alpha_{oi}\partial \alpha_{oi}}|_0\end{bmatrix}
\end{aligned} \tag{103}
$$

The first-order partial derivative of Eq. (19) is given by

$$
\frac{\partial {}^{b}\boldsymbol{p}_{\kappa fi}(\boldsymbol{q}_{di})}{\partial \boldsymbol{q}_{di}^{T}}\left[\frac{\partial \boldsymbol{q}_{di}(\boldsymbol{\varepsilon},\alpha_{oi})}{\partial \boldsymbol{\varepsilon}^{T}},\frac{\partial \boldsymbol{q}_{di}(\boldsymbol{\varepsilon},\alpha_{oi})}{\partial \alpha_{oi}}\right]=\left[\frac{\partial {}^{b}\boldsymbol{p}_{\kappa fi}(\boldsymbol{\varepsilon},\alpha_{oi})}{\partial \boldsymbol{\varepsilon}^{T}},\frac{\partial {}^{b}\boldsymbol{p}_{\kappa fi}(\boldsymbol{\varepsilon},\alpha_{oi})}{\partial \alpha_{oi}}\right] \tag{104}
$$

By using Eqs. (99) and (102), we have

$$
\frac{\partial {}^{b}\boldsymbol{p}_{\kappa fi}(\boldsymbol{\varepsilon},\alpha_{oi})}{\partial x}|_0={}^{b}R_o\boldsymbol{u}_1,\ \frac{\partial {}^{b}\boldsymbol{p}_{\kappa fi}(\boldsymbol{\varepsilon},\alpha_{oi})}{\partial y}|_0={}^{b}R_o\boldsymbol{u}_2
$$

$$
\frac{\partial {}^{b}\boldsymbol{p}_{\kappa fi}(\boldsymbol{\varepsilon},\alpha_{oi})}{\partial \zeta}|_0={}^{b}R_o\Omega{}^{o}\boldsymbol{p}_{\kappa fi}=\{{}^{o}\boldsymbol{p}_{\kappa fi}\otimes {}^{o}R_b\}^{T}
$$

$$
\frac{\partial {}^{b}\boldsymbol{p}_{\kappa fi}(\boldsymbol{\varepsilon},\alpha_{oi})}{\partial \alpha_{oi}}|_0=-\kappa_{oi}{}^{b}R_{\kappa fi}\Omega^{\kappa fi}\boldsymbol{p}_{\kappa oi}=-\kappa_{oi}\{{}^{\kappa fi}\boldsymbol{p}_{\kappa oi}\otimes {}^{\kappa fi}R_b\}^{T} \tag{105}
$$

Considering the initial condition, Eq. (104) is transformed to

$$
\begin{bmatrix}\dfrac{\partial \boldsymbol{q}_{di}^{T}(\boldsymbol{\varepsilon},\alpha_{oi})}{\partial \boldsymbol{\varepsilon}}|_0\\ \dfrac{\partial \boldsymbol{q}_{di}^{T}(\boldsymbol{\varepsilon},\alpha_{oi})}{\partial \alpha_{oi}}|_0\end{bmatrix}=\begin{bmatrix}W_{\kappa fi}\\ -\kappa_{oi}{}^{\kappa fi}\boldsymbol{p}_{\kappa oi}\otimes {}^{\kappa fi}R_b\end{bmatrix}{}^{b}J_{\kappa fi}^{-T} \tag{106}
$$

From the second-order partial derivative of Eq. (19), we have

$$\begin{bmatrix} \dfrac{\partial^2\{\boldsymbol{u}_k^T[{}^bJ_{\kappa fi}]\boldsymbol{q}_{di}(\boldsymbol{\varepsilon},\alpha_{oi})\}}{\partial\boldsymbol{\varepsilon}\partial\boldsymbol{\varepsilon}^T}|_0 & \dfrac{\partial^2\{\boldsymbol{u}_k^T[{}^bJ_{\kappa fi}]\boldsymbol{q}_{di}(\boldsymbol{\varepsilon},\alpha_{oi})\}}{\partial\boldsymbol{\varepsilon}\partial\alpha_{oi}}|_0 \\ \dfrac{\partial^2\{\boldsymbol{u}_k^T[{}^bJ_{\kappa fi}]\boldsymbol{q}_{di}(\boldsymbol{\varepsilon},\alpha_{oi})\}}{\partial\alpha_{oi}\partial\boldsymbol{\varepsilon}^T}|_0 & \dfrac{\partial^2\{\boldsymbol{u}_k^T[{}^bJ_{\kappa fi}]\boldsymbol{q}_{di}(\boldsymbol{\varepsilon},\alpha_{oi})\}}{\partial\alpha_{oi}\partial\alpha_{oi}}|_0 \end{bmatrix}$$
$$= \begin{bmatrix} \dfrac{\partial^2\{{}^b\boldsymbol{p}_{\kappa fi}^T(\boldsymbol{\varepsilon},\alpha_{oi})\boldsymbol{u}_k\}}{\partial\boldsymbol{\varepsilon}\partial\boldsymbol{\varepsilon}^T}|_0 & \dfrac{\partial^2\{{}^b\boldsymbol{p}_{\kappa fi}^T(\boldsymbol{\varepsilon},\alpha_{oi})\boldsymbol{u}_k\}}{\partial\boldsymbol{\varepsilon}\partial\alpha_{oi}}|_0 \\ \dfrac{\partial^2\{{}^b\boldsymbol{p}_{\kappa fi}^T(\boldsymbol{\varepsilon},\alpha_{oi})\boldsymbol{u}_k\}}{\partial\alpha_{oi}\partial\boldsymbol{\varepsilon}^T}|_0 & \dfrac{\partial^2\{{}^b\boldsymbol{p}_{\kappa fi}^T(\boldsymbol{\varepsilon},\alpha_{oi})\boldsymbol{u}_k\}}{\partial\alpha_{oi}\partial\alpha_{oi}}|_0 \end{bmatrix} \tag{107}$$
$$- \begin{bmatrix} \dfrac{\partial\boldsymbol{q}_{di}^T(\boldsymbol{\varepsilon},\alpha_{oi})}{\partial\boldsymbol{\varepsilon}}|_0 \\ \dfrac{\partial\boldsymbol{q}_{di}^T(\boldsymbol{\varepsilon},\alpha_{oi})}{\partial\alpha_{oi}}|_0 \end{bmatrix} \begin{bmatrix} \dfrac{\partial\{{}^b\boldsymbol{p}_{\kappa fi}^T(\boldsymbol{q}_{di})\boldsymbol{u}_k\}}{\partial\boldsymbol{q}_{di}\partial\boldsymbol{q}_{di}^T}|_0 \end{bmatrix} \begin{bmatrix} \dfrac{\partial\boldsymbol{q}_{di}^T(\boldsymbol{\varepsilon},\alpha_{oi})}{\partial\boldsymbol{\varepsilon}}|_0 \\ \dfrac{\partial\boldsymbol{q}_{di}^T(\boldsymbol{\varepsilon},\alpha_{oi})}{\partial\alpha_{oi}}|_0 \end{bmatrix}^T$$

According to Eqs. (99) and (102), we have

$$\frac{\partial^b\boldsymbol{p}_{\kappa fi}(\boldsymbol{\varepsilon},\alpha_{oi})}{\partial\alpha_{oi}\partial\zeta}|_0 = -\kappa_{oi}\,{}^bR_{\kappa oi}\,{}^{\kappa oi}\boldsymbol{p}_{\kappa fi} = \kappa_{oi}\,{}^bR_{\kappa fi}\,{}^{\kappa fi}\boldsymbol{p}_{\kappa oi} \tag{108}$$

The other elements are obtained in a similar manner. The last term of Eq. (103) is obtained by replacing $\boldsymbol{u}_k$ with ${}^b\boldsymbol{f}_{\kappa fi} = {}^bJ_{\kappa fi}^{-T}\boldsymbol{\tau}_i$.

If the object's surface is flat, we have

$$\lim_{\kappa_{oi}\to 0}\kappa_{oi}\,{}^{\kappa fi}\boldsymbol{p}_{\kappa oi} = \boldsymbol{u}_1, \quad \lim_{\kappa_{oi}\to 0}\kappa_{oi}^2\{{}^{\kappa fi}\boldsymbol{p}_{\kappa oi}\} = 0 \tag{109}$$

where ${}^{\kappa fi}\boldsymbol{p}_{\kappa oi} = (\kappa_{oi}^{-1} + \kappa_{fi}^{-1})\boldsymbol{u}_1$ from Eq. (12). These equations are used in Eqs. (22)-(23).

Appendix B: Gradient and Hessian with a Contact Condition

Differentiating Eqs. (30) and (43) yield

$$G_i^{fc} = \frac{\partial U_i^{fc}(\boldsymbol{\varepsilon})}{\partial\boldsymbol{\varepsilon}}|_0 = [I_3, Q_i^{fc}]\begin{bmatrix} U_{i,\varepsilon} \\ U_{i,\alpha} \end{bmatrix}$$
$$H_i^{fc} = \frac{\partial^2 U_i^{fc}(\boldsymbol{\varepsilon})}{\partial\boldsymbol{\varepsilon}\partial\boldsymbol{\varepsilon}^T}|_0 = [I_3, Q_i^{fc}]\begin{bmatrix} U_{i,\varepsilon\varepsilon} & U_{i,\alpha\varepsilon} \\ U_{i,\varepsilon\alpha} & U_{i,\alpha\alpha} \end{bmatrix}[I_3, Q_i^{fc}]^T + U_{i,\alpha}\frac{\partial^2\alpha_{oi}^{fc}(\boldsymbol{\varepsilon})}{\partial\boldsymbol{\varepsilon}\partial\boldsymbol{\varepsilon}^T}|_0 \tag{110}$$

where

$$Q_i^{fc} = \frac{\partial\alpha_{oi}^{fc}(\boldsymbol{\varepsilon})}{\partial\boldsymbol{\varepsilon}}|_0 \in \mathbb{R}^3 \tag{111}$$

Appendix C: Derivation of Eqs. (31)-(32)

From Eqs. (27) and (29), $\boldsymbol{\varepsilon}$ satisfies

$$\frac{\partial U_i(\boldsymbol{\varepsilon},\alpha_{oi}^{fs}(\boldsymbol{\varepsilon}))}{\partial\alpha_{oi}} = 0 \tag{112}$$

Hence, we have

$$\frac{\partial}{\partial\boldsymbol{\varepsilon}}\left[\frac{\partial U_i(\boldsymbol{\varepsilon},\alpha_{oi}^{fs}(\boldsymbol{\varepsilon}))}{\partial\alpha_{oi}}\right] = \frac{\partial^2 U_i(\boldsymbol{\varepsilon},\alpha_{oi})}{\partial\boldsymbol{\varepsilon}\partial\alpha_{oi}} + \left(\frac{\partial\alpha_{oi}^{fs}(\boldsymbol{\varepsilon})}{\partial\boldsymbol{\varepsilon}}\right)\frac{\partial U_i(\boldsymbol{\varepsilon},\alpha_{oi})}{\partial\alpha_{oi}\partial\alpha_{oi}} = 0 \tag{113}$$

Considering the initial condition, we have

$$Q_i^{fs} = \frac{\partial \alpha_{oi}^{fs}(\boldsymbol{\varepsilon})}{\partial \boldsymbol{\varepsilon}}|_0 = -U_{i,\alpha\varepsilon}U_{i,\alpha\alpha}^{-1} \tag{114}$$

From Eq. (27), we have $U_{i,\alpha} = 0$. Then, Eq. (110) is transformed to

$$G_i^{fs} = [I_3, -U_{i,\alpha\varepsilon}U_{i,\alpha\alpha}^{-1}]\begin{bmatrix} U_{i,\varepsilon} \\ U_{i,\alpha} \end{bmatrix} = U_{i,\varepsilon}$$

$$H_i^{fs} = [I_3, -U_{i,\alpha\varepsilon}U_{i,\alpha\alpha}^{-1}]\begin{bmatrix} U_{i,\varepsilon\varepsilon} & U_{i,\alpha\varepsilon} \\ U_{i,\varepsilon\alpha} & U_{i,\alpha\alpha} \end{bmatrix}[I_3, -U_{i,\alpha\varepsilon}U_{i,\alpha\alpha}^{-1}]^T = U_{i,\varepsilon\varepsilon} - U_{i,\alpha\varepsilon}U_{i,\alpha\alpha}^{-1}U_{i,\varepsilon\alpha} \tag{115}$$

Appendix D: Effect of Change in the Local Curvature in a Frictionless Sliding Contact Case

From Eq. (115), the matrix is rewritten by

$$H_i^{fs} = U_{i,\varepsilon\varepsilon} - V_{i,\alpha\varepsilon}V_{i,\alpha\alpha}^{-1}V_{i,\varepsilon\alpha} \tag{116}$$

where

$$V_{i,\alpha\varepsilon} = \frac{U_{i,\alpha\varepsilon}}{\kappa_{oi}(\kappa_{oi}^{-1} + \kappa_{fi}^{-1})} = c_1\boldsymbol{v}_\zeta - \boldsymbol{a}_1$$

$$V_{i,\alpha\alpha} = \frac{U_{i,\alpha\alpha}}{\{\kappa_{oi}(\kappa_{oi}^{-1} + \kappa_{fi}^{-1})\}^2} = \frac{c_1}{\kappa_{oi}^{-1} + \kappa_{fi}^{-1}} + c_2$$

$$Q_i^{fs} = -\frac{V_{i,\alpha\varepsilon}V_{i,\alpha\alpha}^{-1}}{\kappa_{oi}(\kappa_{oi}^{-1} + \kappa_{fi}^{-1})}, \quad c_1 = {}^b\boldsymbol{f}_{\kappa fi}^T\,{}^bR_{\kappa fi}\boldsymbol{u}_1$$

$$c_2 = \boldsymbol{u}_2^{T\,\kappa fi}R_b\,{}^bJ_{\kappa fi}^{-T}\{S_i - S_{\kappa fi}\}\,{}^bJ_{\kappa fi}^{-1}\{{}^bR_{\kappa fi}\}\boldsymbol{u}_2$$

$$\boldsymbol{a}_1 = W_{\kappa fi}\,{}^bJ_{\kappa fi}^{-T}\{S_i - S_{\kappa fi}\}\,{}^bJ_{\kappa fi}^{-1}\{{}^bR_{\kappa fi}\}\boldsymbol{u}_2 \tag{117}$$

The partial derivatives of Eq. (115) by object curvature are given by

$$\frac{\partial G_i^{fs}}{\partial \kappa_{oi}} = \frac{\partial W_{\kappa fi}}{\partial \kappa_{oi}}\,{}^b\boldsymbol{f}_{\kappa fi} + W_{\kappa fi}\frac{\partial\,{}^b\boldsymbol{f}_{\kappa fi}}{\partial \kappa_{oi}} = 0$$

$$\begin{aligned}\frac{\partial H_i^{fs}}{\partial \kappa_{oi}} &= \frac{\partial U_{i,\varepsilon\varepsilon}}{\partial \kappa_{oi}} - V_{i,\alpha\varepsilon}\frac{\partial V_{i,\alpha\alpha}^{-1}}{\partial \kappa_{oi}}V_{i,\varepsilon\alpha} - \frac{\partial V_{i,\alpha\varepsilon}}{\partial \kappa_{oi}}V_{i,\alpha\alpha}^{-1}V_{i,\varepsilon\alpha} - V_{i,\alpha\varepsilon}V_{i,\alpha\alpha}^{-1}\frac{\partial V_{i,\varepsilon\alpha}}{\partial \kappa_{oi}} \\ &= \frac{\partial U_{i,\varepsilon\varepsilon}}{\partial \kappa_{oi}} + \{\kappa_{oi}(\kappa_{oi}^{-1} + \kappa_{fi}^{-1})\}^2 Q_i^{fs}\frac{\partial V_{i,\alpha\alpha}}{\partial \kappa_{oi}}\{Q_i^{fs}\}^T - \kappa_{oi}(\kappa_{oi}^{-1} + \kappa_{fi}^{-1})\left\{\frac{\partial V_{i,\alpha\varepsilon}}{\partial \kappa_{oi}}\{Q_i^{fs}\}^T + Q_i^{fs}\frac{\partial V_{i,\varepsilon\alpha}}{\partial \kappa_{oi}}\right\} \\ &= c_1 Q_i^{fs}\{Q_i^{fs}\}^T\end{aligned} \tag{118}$$

where

$$\frac{\partial U_{i,\varepsilon\varepsilon}}{\partial \kappa_{oi}} = 0, \quad \frac{\partial V_{i,\alpha\varepsilon}}{\partial \kappa_{oi}} = 0, \frac{\partial V_{i,\alpha\alpha}}{\partial \kappa_{oi}} = \frac{c_1}{\{\kappa_{oi}(\kappa_{oi}^{-1} + \kappa_{fi}^{-1})\}^2} \tag{119}$$

The partial derivatives by finger curvature are given by

$$\frac{\partial\,{}^o\boldsymbol{p}_{\kappa fi}}{\partial \kappa_{fi}} = \frac{\partial\{{}^o\boldsymbol{p}_{Lfi} + {}^oR_{Lfi}\,{}^{Lfi}\boldsymbol{p}_{\kappa fi}\}}{\partial \kappa_{fi}} = \kappa_{fi}^{-2}\{{}^oR_{Lfi}\}\boldsymbol{u}_1$$

$$\frac{\partial W_{\kappa fi}}{\partial \kappa_{fi}} = \frac{\partial\{W_{Lfi} - \kappa_{fi}^{-1}\boldsymbol{v}_\zeta\boldsymbol{u}_2^T[{}^{Lfi}R_b]\}}{\partial \kappa_{fi}} = \kappa_{fi}^{-2}\boldsymbol{v}_\zeta\boldsymbol{u}_2^T\{{}^{Lfi}R_b\}$$

$$\frac{\partial\,{}^b\boldsymbol{f}_{\kappa fi}}{\partial \kappa_{fi}} = \frac{\partial\,{}^bJ_{\kappa fi}^{-T}}{\partial \kappa_{fi}}\boldsymbol{\tau}_i = -{}^bJ_{\kappa fi}^{-T}\frac{\partial\,{}^bJ_{\kappa fi}^T}{\partial \kappa_{fi}}\,{}^bJ_{\kappa fi}^{-T}\boldsymbol{\tau}_i = 0$$

$$\frac{\partial U_{i,\varepsilon\varepsilon}}{\partial \kappa_{fi}} = \kappa_{fi}^{-2}\{\boldsymbol{a}_2 V_{i,\alpha\varepsilon}^T + V_{i,\alpha\varepsilon}\boldsymbol{a}_2^T + c_1\boldsymbol{a}_2\boldsymbol{a}_2^T\}$$

$$\frac{\partial V_{i,\alpha\varepsilon}}{\partial \kappa_{fi}} = -\kappa_{fi}^{-2}\{(c_1c_3 - c_2)\boldsymbol{a}_2 + c_3 V_{i,\alpha\varepsilon}\}$$

$$\frac{\partial V_{i,\alpha\alpha}}{\partial \kappa_{fi}} = \kappa_{fi}^{-2}\{-2c_2c_3 + c_1c_3^2 + c_1(\kappa_{oi}^{-1} + \kappa_{fi}^{-1})^{-2}\}$$

$$c_3 = \boldsymbol{u}_2^T {}^{\kappa fi}R_b\, {}^bJ_{\kappa fi}^{-T}\boldsymbol{c}_q, \quad \boldsymbol{a}_2 = W_{\kappa fi}\, {}^bJ_{\kappa fi}^{-T}\boldsymbol{c}_q - \boldsymbol{v}_\zeta \tag{120}$$

For the revolute joint case,

$$\frac{\partial\, {}^bJ_{\kappa fi}}{\partial \kappa_{fi}} = \frac{\partial\{{}^bJ_{Lfi} - \kappa_{fi}^{-1}\{{}^bR_{Lfi}\}\boldsymbol{u}_2[1,1]\}}{\partial \kappa_{fi}} = \kappa_{fi}^{-2}\{{}^bR_{Lfi}\}\boldsymbol{u}_2[1,1]$$

$$\frac{\partial S_{\kappa fi}}{\partial \kappa_{fi}} = -\kappa_{fi}^{-2}c_1\begin{bmatrix}1\\1\end{bmatrix}[1,1] \tag{121}$$

For the prismatic joint case,

$$\frac{\partial^b J_{\kappa fi}}{\partial \kappa_{fi}} = 0_{2\times 2}, \quad \frac{\partial S_{\kappa fi}}{\partial \kappa_{fi}} = 0_{2\times 2} \tag{122}$$

Finally, we have

$$\frac{\partial H_i^{fs}}{\partial \kappa_{fi}} = \frac{c_1}{\kappa_{fi}^2}\left\{\boldsymbol{a}_2 + \left(\frac{1}{\kappa_{oi}^{-1} + \kappa_{fi}^{-1}} + c_3\right)\frac{V_{i,\alpha\varepsilon}}{V_{i,\alpha\alpha}}\right\}\left\{\boldsymbol{a}_2 + \left(\frac{1}{\kappa_{oi}^{-1} + \kappa_{fi}^{-1}} + c_3\right)\frac{V_{i,\alpha\varepsilon}}{V_{i,\alpha\alpha}}\right\}^T = c_1\boldsymbol{b}_i^{fs}\{\boldsymbol{b}_i^{fs}\}^T \tag{123}$$

Appendix E: Derivation in the Grasp Stiffness Matrix with Rolling Contact

The first- and second-order partial derivatives of Eq. (43) are obtained from

$$G_i^{fr} = \frac{\partial U_i^{fr}(\boldsymbol{\varepsilon})}{\partial \boldsymbol{\varepsilon}}|_0 = \left[\frac{\partial\{\boldsymbol{q}_{di}^{fr}(\boldsymbol{\varepsilon})\}^T}{\partial \boldsymbol{\varepsilon}}|_0\right]\boldsymbol{\tau}_i$$

$$H_i^{fr} = \frac{\partial^2 U_i^{fr}(\boldsymbol{\varepsilon})}{\partial \boldsymbol{\varepsilon}\partial \boldsymbol{\varepsilon}^T}|_0 = \left[\frac{\partial\{\boldsymbol{q}_{di}^{fr}(\boldsymbol{\varepsilon})\}^T}{\partial \boldsymbol{\varepsilon}}|_0\right]S_i\left[\frac{\partial\{\boldsymbol{q}_{di}^{fr}(\boldsymbol{\varepsilon})\}^T}{\partial \boldsymbol{\varepsilon}}|_0\right]^T + \frac{\partial\{\boldsymbol{\tau}_i^T\boldsymbol{q}_{di}^{fr}(\boldsymbol{\varepsilon})\}}{\partial \boldsymbol{\varepsilon}\partial \boldsymbol{\varepsilon}^T}|_0 \tag{124}$$

From the first-order partial derivative of Eq. (41), we have

$$\frac{\partial\{\boldsymbol{q}_{di}^{fr}(\boldsymbol{\varepsilon})\}^T}{\partial \boldsymbol{\varepsilon}}|_0 = W_{Lfi}\, {}^bJ_{Lfi}^{-T} \tag{125}$$

Calculating the second-order partial derivative of Eq. (41) and considering the initial condition, we have

$$\begin{aligned}&\frac{\partial^2\{\boldsymbol{\tau}_i^T\boldsymbol{q}_{di}^{fr}(\boldsymbol{\varepsilon})\}}{\partial \boldsymbol{\varepsilon}\partial \boldsymbol{\varepsilon}^T}|_0\\ &= -\{{}^b\boldsymbol{f}_{Lfi}^T\, {}^bR_o\, {}^o\boldsymbol{p}_{Lfi}\}\boldsymbol{v}_\zeta\boldsymbol{v}_\zeta^T - \{W_{Lfi}\, {}^bJ_{Lfi}^{-T}\}S_{Lfi}\{W_{Lfi}\, {}^bJ_{Lfi}^{-T}\}^T\\ &- \frac{{}^b\boldsymbol{f}_{Lfi}^T\, {}^bR_{Lfi}\boldsymbol{u}_1}{\kappa_{oi} + \kappa_{fi}}\{W_{Lfi}\, {}^bJ_{Lfi}^{-T}\boldsymbol{c}_q - \boldsymbol{v}_\zeta\}\{W_{Lfi}\, {}^bJ_{Lfi}^{-T}\boldsymbol{c}_q - \boldsymbol{v}_\zeta\}^T\end{aligned} \tag{126}$$

In section 5, the gradient and Hessian of Eq. (43) are obtained without the reduction of α_{fi} to simplify the derivation. The same gradient and Hessian are also obtained from Appendix B considering

$$Q_i^{fr} = \frac{\partial \alpha_{oi}^{fr}(\boldsymbol{\varepsilon})}{\partial \boldsymbol{\varepsilon}}|_0 = \frac{1}{\kappa_{oi} + \kappa_{fi}}\left\{\frac{\partial\{\boldsymbol{c}_q^T\boldsymbol{q}_{di}^{fr}(\boldsymbol{\varepsilon})\}}{\partial \boldsymbol{\varepsilon}}|_0 - \boldsymbol{v}_\zeta\right\}$$

$$\frac{\partial^2 \alpha_{oi}^{fr}(\boldsymbol{\varepsilon})}{\partial \boldsymbol{\varepsilon} \partial \boldsymbol{\varepsilon}^T}|_0 = \frac{1}{\kappa_{oi}+\kappa_{fi}}\left[\frac{\partial^2 \{\boldsymbol{c}_q^T \boldsymbol{q}_{di}^{fr}(\boldsymbol{\varepsilon})\}}{\partial \boldsymbol{\varepsilon} \partial \boldsymbol{\varepsilon}^T}|_0\right] \tag{127}$$

Eq. (53) is obtained from Eq. (125) and the first equation of (127). By replacing ${}^b J_{Lfi}^T \boldsymbol{u}_k$ with $\boldsymbol{c}_q$, the second equation can be transformed.

Appendix F: Difference between the Stiffness Matrix in the Revolute Joint and Prismatic Joint Cases

The stiffness matrix with prismatic stiffness is given by

$$H_i^{fr} = \{W_{Lfi}\,{}^b R_{Lfi}\} S_{pi}^{fr} \{W_{Lfi}\,{}^b R_{Lfi}\}^T - \left\{ {}^b \boldsymbol{f}_{Lfi}^T\, {}^b R_o\, {}^o \boldsymbol{p}_{Lfi} - \frac{{}^b \boldsymbol{f}_{Lfi}^T\, {}^b R_{Lfi} \boldsymbol{u}_1}{\kappa_{oi}+\kappa_{fi}} \right\} \boldsymbol{v}_\zeta \boldsymbol{v}_\zeta^T \tag{128}$$

where S_{pi}^{fr} denotes the prismatic stiffness to distinguish it from the revolute stiffness S_i. The difference between Eqs. (45) and (128) is given by

$$H_{di}^{fr} = W_{Lfi}[{}^b J_{Lfi}^{-T}\{S_i - S_{Lfi}\}\,{}^b J_{Lfi}^{-1} - {}^b R_{Lfi}\{S_{pi}^{fr}\}^{Lfi} R_b] W_{Lfi}^T + \frac{{}^b \boldsymbol{f}_{Lfi}^T\, {}^b R_{Lfi} \boldsymbol{u}_1}{\kappa_{oi}+\kappa_{fi}} [\boldsymbol{v}_\zeta \boldsymbol{v}_\zeta^T - \{W_{Lfi}\,{}^b J_{Lfi}^{-T} \boldsymbol{c}_q - \boldsymbol{v}_\zeta\}\{W_{Lfi}\,{}^b J_{Lfi}^{-T} \boldsymbol{c}_q - \boldsymbol{v}_\zeta\}^T] \tag{129}$$

If Eq. (49) is used, we have Eq. (50).

Appendix G: Difference between Rolling and Sliding Grasp Stiffness Matrices

In the case of $U_{i,\alpha} = 0$, the difference between the rolling and the sliding stiffness matrices is obtained as

$$\begin{aligned} H_i^{fd} &= H_i^{fr} - H_i^{fs} = U_{i,\varepsilon\varepsilon} + Q_i^{fr} U_{i,\varepsilon\alpha} + U_{i,\alpha\varepsilon}\{Q_i^{fr}\}^T + Q_i^{fr} U_{i,\alpha\alpha}\{Q_i^{fr}\}^T - \{U_{i,\varepsilon\varepsilon} - U_{i,\alpha\varepsilon} U_{i,\alpha\alpha}^{-1} U_{i,\varepsilon\alpha}\} \\ &= U_{i,\alpha\alpha}\{Q_i^{fr} + U_{i,\alpha\varepsilon} U_{i,\alpha\alpha}^{-1}\}\{Q_i^{fr} + U_{i,\alpha\varepsilon} U_{i,\alpha\alpha}^{-1}\}^T = U_{i,\alpha\alpha}\{Q_i^{fr} - Q_i^{fs}\}\{Q_i^{fr} - Q_i^{fs}\}^T \end{aligned} \tag{130}$$

Appendix H: Case of Finger with Both Prismatic and Revolute Joints

In the case that the first joint is a prismatic type and the second joint is a revolute type, we obtain

$$\begin{aligned} c_q^T &= [0,1], \quad {}^b J_{\kappa fi} = [{}^b R_{i1}\boldsymbol{u}_1, {}^b R_{i2}\Omega^{i2}\boldsymbol{p}_{\kappa fi}] \\ S_{\kappa fi} &= -{}^b \boldsymbol{f}_{\kappa fi}^T\, {}^b R_{i2}\, {}^{i2}\boldsymbol{p}_{\kappa fi} \begin{bmatrix} 0 & 0 \\ 0 & 1 \end{bmatrix} \\ {}^b J_{Lfi} &= [{}^b R_{i1}\boldsymbol{u}_1, {}^b R_{i2}\Omega^{i2}\boldsymbol{p}_{Lfi}] \\ S_{Lfi} &= -{}^b \boldsymbol{f}_{Lfi}^T\, {}^b R_{i2}\, {}^{i2}\boldsymbol{p}_{Lfi} \begin{bmatrix} 0 & 0 \\ 0 & 1 \end{bmatrix} \end{aligned} \tag{131}$$

In the case that the first joint is a revolute type and the second joint is a prismatic type, we obtain

$$\begin{aligned} c_q^T &= [1,0], \quad {}^b J_{\kappa fi} = [{}^b R_{i1}\Omega^{i1}\boldsymbol{p}_{\kappa fi}, {}^b R_{i2}\boldsymbol{u}_1] \\ S_{\kappa fi} &= -{}^b \boldsymbol{f}_{\kappa fi}^T\, {}^b R_{i1}\, {}^{i1}\boldsymbol{p}_{\kappa fi} \begin{bmatrix} 1 & 0 \\ 0 & 0 \end{bmatrix} + {}^b \boldsymbol{f}_{\kappa fi}^T\, {}^b R_{i2}\boldsymbol{u}_2 \begin{bmatrix} 0 & 1 \\ 1 & 0 \end{bmatrix} \\ {}^b J_{Lfi} &= [{}^b R_{i1}\Omega^{i1}\boldsymbol{p}_{Lfi}, {}^b R_{i2}\boldsymbol{u}_1] \\ S_{Lfi} &= -{}^b \boldsymbol{f}_{Lfi}^T\, {}^b R_{i1}\, {}^{i1}\boldsymbol{p}_{Lfi} \begin{bmatrix} 1 & 0 \\ 0 & 0 \end{bmatrix} + {}^b \boldsymbol{f}_{Lfi}^T\, {}^b R_{i2}\boldsymbol{u}_2 \begin{bmatrix} 0 & 1 \\ 1 & 0 \end{bmatrix} \end{aligned} \tag{132}$$